NTIA Report 01-384

Measurements to Determine Potential Interference to GPS Receivers from Ultrawideband Transmission Systems

J. Randy Hoffman
Michael G. Cotton
Robert J. Achatz
Richard N. Statz
Roger A. Dalke

U.S. DEPARTMENT OF COMMERCE
Donald L. Evans, Secretary

John F. Sopko, Acting Assistant Secretary
for Communications and Information

February 2001

This Page Intentionally Left Blank

This Page Intentionally Left Blank

Product Disclaimer

Certain commercial equipment, instruments, or materials are identified in this report to specify the technical aspects of the reported results. In no case does such identification imply recommendation or endorsement by the National Telecommunications and Information Administration, nor does it imply that the material or equipment identified is necessarily the best available for the purpose.

This Page Intentionally Left Blank

This Page Intentionally Left Blank

CONTENTS

MEASUREMENTS TO DETERMINE POTENTIAL INTERFERENCE TO GPS RECEIVERS FROM ULTRAWIDEBAND TRANSMISSION SYSTEMS

J. Randy Hoffman, Michael G. Cotton, Robert J. Achatz,
Richard N. Statz, and Roger A. Dalke*

This report describes laboratory measurements of Global Positioning System (GPS) receiver vulnerability to ultrawideband (UWB) interference. The laboratory measurements were performed by inserting increased levels of UWB interference until an operating GPS receiver lost lock. At each interference level leading up to loss of lock, reacquisition time, fundamental GPS measurements (e.g., pseudorange and carrier phase), status flags (e.g., potential cycle slips), and position data were sampled. A variety of UWB signals were tested, including aggregates of as many as six UWB sources. Two GPS receivers with different receiver architectures were tested.

Key words: Global Positioning System (GPS), Ultrawideband (UWB), Impulse Radio, Amplitude Probability Distribution (APD), Interference Measurement, Noise, Radio Frequency Interference (RFI)

1. INTRODUCTION

As new wireless applications and technologies continue to develop, conflicts in spectrum use and system incompatibility are inevitable. This report investigates potential interference to Global Positioning System (GPS) receivers by ultrawideband (UWB) signals. According to Part 15 of the Federal Communications Commission (FCC) rules, non-licensed operation of low-power transmitters is allowed if interference to licensed radio systems is negligible. On May 11, 2000, the FCC issued a Notice of Proposed Rulemaking (NPRM) [1] which proposed that UWB devices operate under Part 15 rules. This would exempt UWB systems from licensing and frequency coordination and allow them to operate under a new UWB section of Part 15, based on claims that UWB devices can operate on spectrum already occupied by existing radio services without causing interference. The NPRM calls for further testing and analysis, so that risks of UWB interference are understood and critical radio services, particularly safety services such as GPS, are adequately protected.

Conventional methods of measuring and quantifying interference under narrowband assumptions are insufficient for testing UWB interference. Recently, NTIA's Institute for Telecommunication Sciences (ITS) investigated general characteristics of UWB signals [2]. As a natural extension to the UWB characterization study, this investigation measures the interference from a representative set of UWB signals imposed on a select group of GPS

* The authors are with the Institute for Telecommunication Sciences, National Telecommunications and Information Administration, U.S. Department of Commerce, Boulder, CO 80303.

receivers. The remainder of this section discusses the relevant technologies and associated applications, briefly summarizes related studies, and gives an outline for this report.

1.1 The Technologies

The multifaceted strategic and commercial importance of GPS and the potential commercial importance of UWB are summarized in the following subsections.

1.1.1 Global Positioning System

The Global Positioning System has emerged as a universal cornerstone for much of our technological infrastructure. GPS is a space-based, broadcast-only, radio navigation satellite service that provides universal access to position, velocity, and time information on a continuous worldwide basis. The GPS constellation consists of twenty-four satellites that transmit encrypted high-precision pseudo-random noise (PRN) codes (i.e., P(Y) codes), used by U.S. and allied military forces, and unencrypted coarse-acquisition PRN codes (i.e., C/A codes), which are used in a myriad of commercial and consumer applications.

GPS is a powerful enabling technology that has created new industries and new industrial practices fully dependent upon GPS signal reception. It is presently used in aviation for en-route and non-precision approach landing phases of flight. Precision-approach services, runway incursion, and ground traffic management are currently being developed. On our highways, GPS assists in vehicle guidance, and monitoring; public safety and emergency response; resource management; collision avoidance; and transit command and control. Non-navigation applications are often grouped into geodesy and surveying; mapping, charting, and geographic information systems; geophysical measurement and monitoring; meteorological applications; and timing and frequency. Planned systems, such as Enhanced 911, personal location, and medical tracking devices are soon to be commercially available. Moreover, the U.S. telecommunications and power distribution systems are also dependent upon GPS for network synchronization timing.

1.1.2 Ultrawideband Transmission Systems

Unlike conventional radio systems, UWB devices bypass intermediate frequency (IF) stages, possibly reducing complexity and cost. Additionally, the high cost of frequency allocation for these devices is avoided if they are allowed to operate under Part 15 rules. These potential advantages have been a catalyst for the development of UWB technologies.

UWB signals are characterized by modulation methods that vary pulse timing and position rather than carrier-frequency, amplitude, or phase. Short pulses (on the order of a nanosecond) spread their power across a wide bandwidth and the power density decreases. UWB proponents argue that the power spectral density decreases below the threshold of narrowband receivers, hence, causing negligible interference. Other advantages are mitigation of frequency selective fading induced by multipath or transmission through materials.

Existing and potential applications for UWB technology can be divided into two groups – wireless communications and short-range sensing. In wireless communications, it has been shown to be an effective way to link many users in multipath environments (e.g., distribution of wireless services throughout a home or office). In short-range sensing applications, it can be used for determining structural soundness of bridges, roads, and runways and locating objects and utilities underground. Potential automotive uses include collision avoidance systems, air bag proximity measurement for safe deployment, and fluid level detectors. UWB technology is being developed for new types of imaging systems that would assist rescue personnel in locating persons hidden behind walls, under debris, or under snow.

1.2 Brief History of GPS versus UWB Compatibility Measurements

There are other measurement efforts underway to assess the potential for compatibility between UWB devices and existing GPS receivers. The Department of Transportation (DOT) has sponsored a GPS/UWB compatibility study at Stanford University, focusing on precision-approach aviation receivers that conform to the minimum operational performance standards. The general test procedure was a conducted experiment and utilized a radio frequency interference (RFI) -equivalence concept to relate the impact of UWB signals on GPS to that of Gaussian noise. A second measurement effort at the Applied Research Laboratories of the University of Texas at Austin (ARL/UT) was sponsored by the Ultra-Wideband Consortium. ARL/UT collected fundamental GPS parameters under conducted, radiated, and live-sky conditions for assessing single- and aggregate-source UWB interference to GPS receivers. Data analysis, however, was left to be performed by the GPS and UWB communities.

1.3 Scope

The objective of this study was to measure the degree of interference to various GPS receivers from different UWB signals. Recommendations on UWB regulation are left to the policy teams at NTIA's Office of Spectrum Management (OSM) and the FCC. These measurements were designed to observe and report on broad trends in GPS performance when subjected to UWB interference. No attempt was made to evaluate specific receiver designs or interference mitigation strategies or provide precise degradation criteria.

1.4 Organization of this Report

Investigation of UWB interference to GPS receivers encompasses a broad range of expertise including GPS theory and operation, radio frequency (RF) design and hardware implementation, automated measurement development, temporal and spectral characterization of interfering signals, and statistical error analysis. This report completely describes the experiment and is organized as follows.

The first three sections provide orientation and background for the reader. Section 2 describes the characteristics of GPS signals, identifies GPS vulnerability to noise and continuous-wave (CW) interference and describes the nature of UWB signals. Section 3 discusses, at a high level, the general methodologies for measuring GPS performance degradation and describes GPS performance metrics.

Section 4 describes the GPS Interference Test Fixture, experimental procedures, categorization of tested GPS receivers, selected UWB signal parameters, calibration details, signal generation, and power settings. Section 5 describes the methods used for analyzing the collected data. Section 6 displays the experimental results which summarize trends in performance degradation. Conclusions are drawn in Section 7.

Appendices are provided for comprehensive purposes and contain supporting information and detailed measurement results. Appendix A is a comparison between radiated and conducted UWB interference tests. Appendix B describes hardware specifications and settings for the RF components of the test fixture, UWB signal generation equipment, and GPS receivers. Appendix C and D provide measured and theoretical characteristics of all the UWB signal types under test. Appendix E is a brief tutorial on the amplitude probability distribution (APD) which is an important method for characterizing UWB signals. Finally, Appendix F contains a complete set of GPS/UWB interference analysis plots.

2. SIGNAL CHARACTERISTICS

The purpose of this section is to describe GPS and UWB signal characteristics in order to identify potential interference scenarios and rationalize measurement procedures.

2.1 GPS

GPS is a spread spectrum system. Each GPS satellite is assigned a unique PRN sequence, and all the PRN codes are nearly uncorrelated with respect to each other; therefore, an individual satellite signal is unique and is distinguished through code division multiple access (CDMA). The signals are transmitted at two frequencies: 1575.42 MHz (L1) and 1227.60 MHz (L2). L1 is quadrature-phase modulated with the C/A code and P(Y) code, and L2 is biphase modulated by the P(Y) code.

Each C/A code has a chipping rate of 1.023 Mchips/s and pseudorandom sequence length of 1023, resulting in a code repetition period of 1 ms. The relatively short periodic nature of the C/A code produces a discrete spectrum with spectral lines spaced 1 kHz apart. Because Gold codes are used to generate the pseudorandom sequences, the spectral envelope deviates slightly from a sinc^2 shape (common to maximal length codes) with a null-to-null main-lobe bandwidth of 2.046 MHz. Each P(Y) code has a chipping rate of 10.23 Mchips/s and a code repetition period of 7 days. The P(Y) code produces a sinc^2 power spectral envelope with a null-to-null main-lobe bandwidth of 20.46 MHz and essentially no spectral lines.

Interference imposed on a GPS receiver can have a number of effects. Gaussian-noise interference has the potential to reduce the signal-to-noise ratio (SNR) to such an extent that the GPS receiver can no longer de-correlate the signal. The effects of narrowband interference are more dependent on the proximity to sensitive C/A-code lines in the GPS spectrum. That is, a relatively weak narrowband interfering signal will have little or no effect on the performance of a GPS receiver unless it aligns with a GPS spectral line; if alignment occurs, then interference can be severe.

2.2 UWB

UWB signals are difficult to define. One definition of UWB signals describes the spectral emissions as having an instantaneous bandwidth of at least 25% of the center frequency. Other names for UWB, or terms associated with it, include: impulse radio, impulse radar, carrierless emission, time-domain processed signal, and others.

Terminology and definitions aside, the UWB signal is, in general, a sequence of narrow pulses sometimes encoded with digital information. UWB signal pulse widths are on the order of 0.2 to 10 ns and longer. Some have an impulse-like shape and others have many zero crossings. One form of modulation is pulse-position modulation (PPM) where, for example, a pulse that is slightly advanced from its nominal position represents a "zero," likewise, a slightly retarded pulse represents a "one." Another form of modulation is on-off keying (OOK) where, for example, an absent pulse represents a "zero." In addition to the modulation scheme, the pulses can be dithered. In other words, the pulse will be randomly located relative to its nominal, periodic location (absolute dithering) or relative to the previous pulse (relative dithering). For example, 50% absolute dithering describes a situation where the pulse is randomly located in the first half of the period following the nominal pulse location. Finally, some UWB systems employ gating. This is a process whereby the pulse train is turned on for some time and off for the remainder of a gating period.

The frequency domain characteristics (emission spectrum) of a UWB signal are dependent on the time-domain characteristics described above. The pulse width generally determines the overall shape – envelope – of the emission spectrum. The bandwidth of the pulse spectrum generally exceeds the reciprocal of the pulse width. If the pulse train is uniformly spaced, the emission spectrum will have a series of lines. If dithering is used, there will be a smooth component of the emission spectrum in addition to the line component. The higher the dithering, the greater the power contained in the smooth component versus the line component. Some types of modulation can also reduce the spectral line amplitude. Band-limiting changes the characteristics of the UWB signal further.

3. GENERAL MEASUREMENT METHODOLOGIES

In principle, interference testing is straightforward. To wit, an interference test is performed by applying a "foreign" signal to an operating receiver while monitoring receiver performance. Any degradation in receiver performance, beyond what can be expected under normal operating conditions, is then attributed to the interference.

Thus, for our tests, the interfering UWB signal must be fully characterized, GPS receiver operation must be defined in a way that can be measured, and receiver performance must be monitored in a way that is meaningful with respect to its intended application. This section explains these measurement methodologies.

3.1 Interference Characterization

In real life, UWB and GPS signals are radiated through space and summed within the GPS receiver antenna. In the laboratory, it is easier to control power levels, outside interference, and measurement repeatability if the signals are conducted through cables and added with a power combiner.

However, if conducted signals are used, it is imperative that conducted and radiated signals are characterized and compared to insure that systematic errors are not introduced. Thus, as part of our testing methodology, spectra and waveforms of radiated and conducted UWB signals were measured and compared. The radiated UWB signal was transmitted within an anechoic chamber and received by a GPS receiver antenna while the conducted UWB signal was transmitted through a coaxial cable connected to a power combiner. Results of this comparison, given in Appendix A, show that differences between radiated and conducted UWB signals are negligible.

There are many different types of UWB signals. The one characteristic they all possess, however, is wide bandwidth. Band-limiting by the GPS receiver significantly alters the characteristics of an already diverse signal set. In the past, engineers have found that the amplitude statistics of the interfering signal have the most bearing on whether it will be benign or destructive to the performance of a victim receiver. Thus, as part of our testing methodology, the amplitude of the UWB signals was sampled and statistically analyzed. Two bandwidths were used, corresponding to the bandwidths of two classes of GPS receivers. Results of this test are provided in Appendix C.

3.2 Operational Testing

An operating GPS receiver must be frequency-locked onto the modulated and Doppler shifted carrier frequency, delay-locked onto the C/A code, and phase-locked onto the message. Thus, at a bare minimum, an operating GPS receiver is frequency-, delay-, and phase-locked to a GPS signal.

Two testing methodologies are used to measure the effect UWB interference has on receiver operation or locking. The break lock (BL) operational test determines the BL point defined to be the minimum amount of interference that causes a receiver to lose lock. The reacquisition time (RQT) operational test determines the amount of time it takes a receiver tracking a GPS signal to reacquire the signal after it has been momentarily removed.

The RQT test does not identify an "RQT point" as the BL test identifies a BL point. It is left to others to determine a reasonable RQT and corresponding RQT point for their application. Once this point is established, the BL and RQT operational tests bracket a region of GPS receiver performance degradation. The RQT point sets the lower bound where the interference begins to have a detrimental effect on the operation of the receiver. The BL point sets the upper bound where operation is impossible.

The BL point may differ significantly from receiver to receiver. For example, surveying receivers require flawless carrier phase-lock. General purpose navigation receivers, however, allow imperfect carrier phase-lock but demand stable C/A code delay-lock, and consequently are more tolerant toward some types of interference.

3.3 Observational Testing

An operating GPS receiver calculates user position through the measurement of GPS "observables." Performance degradation of an operating GPS receiver is commonly evaluated through its observables which include pseudorange, carrier phase, Doppler frequency-shift, clock-offset, signal-to-noise ratio, and carrier cycle-slippage. Observables can usually be obtained from the receiver, in real time, through a computer interface.

Various range estimates are computed from these observables, and errors in the range estimates are subsequently statistically analyzed to determine performance degradation. It is not our intent to use results of this analysis to establish precise range-error budgets. Rather, these statistics are intended to support other trends of UWB interference such as RQT degradation. In addition, range error statistics are useful for isolating performance degradation to C/A code delay-locking or carrier phase-locking functions.

4. MEASUREMENT SYSTEM AND PROCEDURES

The purpose of this section is to provide a detailed summary of the measurement system, test procedures, GPS-receiver and UWB-signal sample space, signal generation details, and hardware limitations for this experiment.

4.1 System

The GPS interference test bed utilized in this experiment was developed at ITS (see Figure 4.1.1). It is comprised of three segments – GPS source, UWB source, and GPS receiver. System configuration is illustrated in Figure 4.1.2 and hardware components are specified in Table 4.1.1 and Appendix B. Each of the contributing signals (i.e., GPS, noise, and UWB) were filtered, amplified, and combined prior to input into the receiver. Signal powers were controlled using precision variable attenuators (VA) controlled by computer. The following subsections provide signal-generation details and justification for hardware employed.

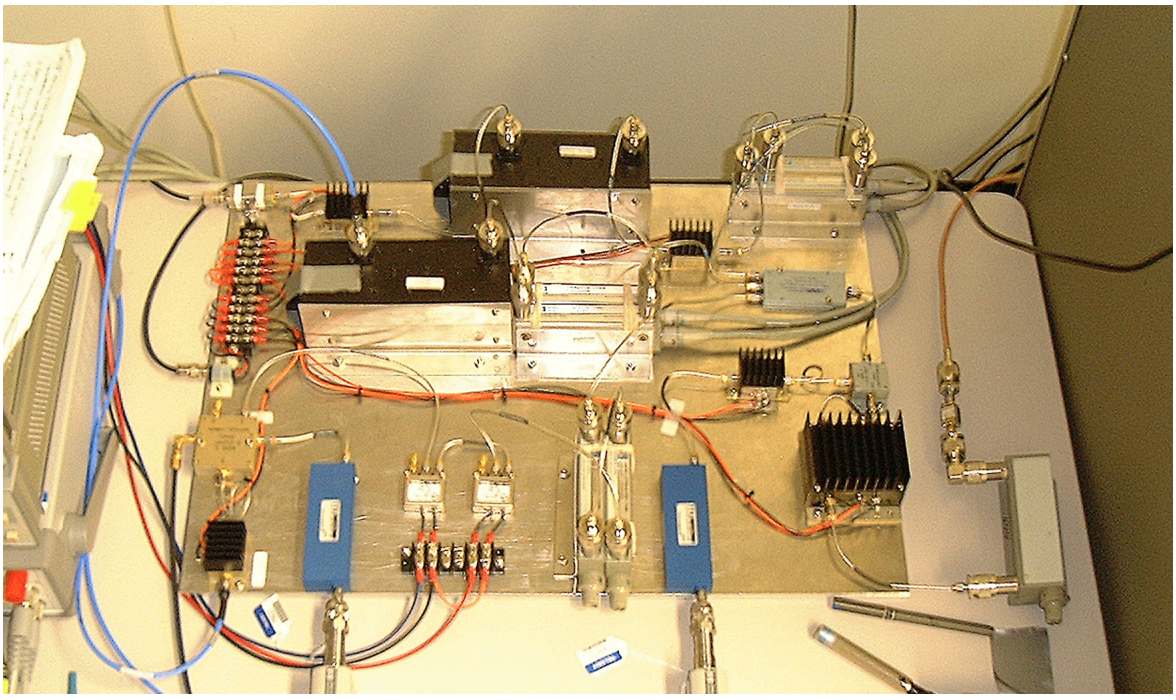

Figure 4.1.1. GPS Interference test bed.

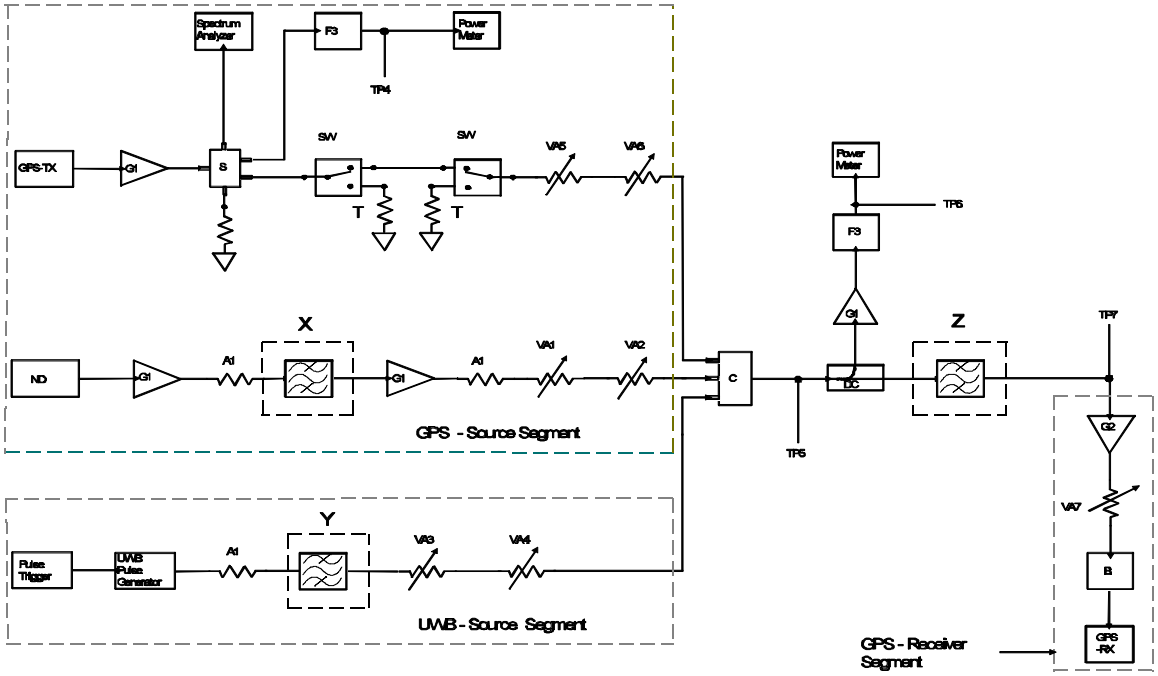

Figure 4.1.2. Block diagram.

Table 4.1.1. Variations in Configuration for Different Receivers

Receiver Description (Rx #)	Noise Diode	Injected Noise[1] (dBm/20MHz)	Fixture[2] X	Fixture Y	Fixture Z
C/A Code (Rx 1)	ND1	-93	F1	F1	Bypassed
Semi-Codeless (Rx 2)	ND2	-120	F2	F2	F4/A2

[1] Gaussian noise power density (dBm/20 MHz) at point TP7 on the test fixture.
[2] Fixtures X, Y, and Z are shown in Figure 4.1.2, and part number are described in Appendix B

4.1.1 GPS-Source Segment

The purpose of the GPS segment is to provide a simulated GPS signal at a known SNR. The GPS signal and background noise were generated with a multi-channel GPS simulator (GPS-TX) and a noise diode (ND), respectively.

Utilization of a GPS simulator provides high-accuracy repetition of scenarios and flexibility for simulation over a wide range of normal and abnormal situations. Generated GPS signals appear as though they had been transmitted from multiple moving satellites, and the simulated satellite positions can be reset to a selected standard configuration at the beginning of each test. Simulated navigation data, required by the user segment and contained in the GPS spread spectrum signal, consists of satellite clock, ephemeris (precise satellite position), and almanac (course satellite position) information.

The GPS simulator used in this experiment is the Nortel model STR2760 provided by the 746th Test Squadron at Holloman Air Force Base. It is the responsibility of the 746th Test Squadron to verify simulator integrity and consistency by comparing simulated signals to measured data; the STR2760 has met those requirements. It reproduces the environment of a GPS receiver installed on a dynamic platform and accounts for receiver and satellite motion and atmospheric effects (e.g., ionospheric delay, tropospheric attenuation and delay, and multipath).

The receiver location was chosen as 32EN, 106EW, and 1000 m above sea level, and the 75-minute scenario was based on an actual constellation beginning on December 16, 1999 at 9:30 p.m. The simulated signals contain Doppler shifts and variable path lengths through the atmosphere according to satellite motion and elevation angle, respectively. Tropospheric attenuation and multipath were turned off. Also, ionospheric delay was simulated only for the receiver with dual-frequency cross-correlation capability.

In this experiment, we focus on the effects of imposed interference. The minimum number of satellites for a receiver to operate nominally, typically four, was chosen. Satellite geometry during the course of the simulation, shown in Figure 4.1.1.1, produces a Position Dilution-of-Precision (PDOP) between 2 and 3. Space vehicle (SV) 25 was chosen as the focus of the experiment. The transmitted signal powers of the other satellites were set to 5 dB greater than that of SV 25. Therefore, under the same interference conditions the SV-25 SNR will be significantly less than the other satellites, and performance degradation will be isolated to the SV-25 channel. Most importantly, as interference is increased the receiver will lose lock on SV 25 first.

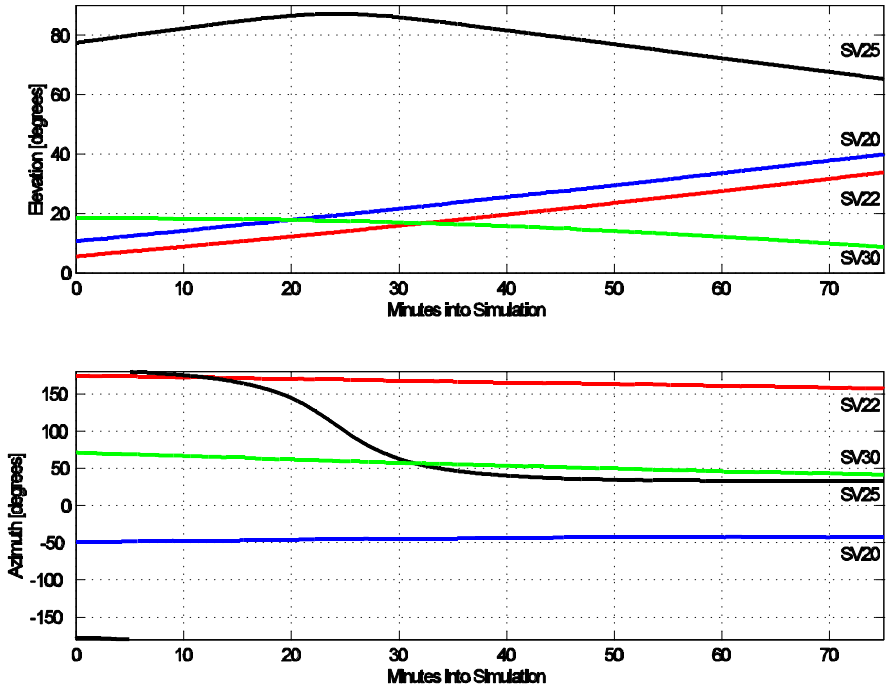

Figure 4.1.1.1. Simulated satellite geometry.

GPS is a CDMA system where multiple transmitters share the same bandwidth. Elevated co-channel interference present with some satellite combinations can produce GPS signal outages. This co-channel interference is approximated with Gaussian noise and emulated with a noise diode in the GPS segment.

4.1.2 UWB-Source Segment

The UWB segment consists of a narrow-pulse generator and a triggering device to create various signals. The pulse shape/width, as a characteristic of the pulse generator, determines the overall spectral envelope. The manner in which the pulses are sequentially spaced (set by the triggering device) determines spectral content within the confines of the envelope. For instance, uniformly spacing the pulses creates strong spectral lines. Dithering the pulse spacing, however, reduces spectral line amplitude and increases noise power density.

The primary criterion for choosing a UWB pulse generator for these measurements depended on whether the spectral envelope was flat and produced sufficient power across the L1 and L2 bands. Two types of UWB pulse generators were utilized, one with a pulse width of 245 ps, and the other with a pulse width of 500 ps. Descriptions of the pulse generators are provided in greater detail in Appendix B. Both pulse generators are triggered by an external device (e.g., arbitrary waveform generator, custom built triggering circuit) to produce different sequential pulse spacings.

For these measurements, the UWB signal is specified by a combination of pulse repetition frequency (PRF), mode of spacing, and the application of gating, all of which have distinctly different effects on spectral and time domain characteristics of the signal.

Four distinct modes of spacing were used: uniform pulse spacing (UPS), on-off keying (OOK), absolute (clock) referenced dithering (ARD), and relative (clock) referenced dithering (RRD). The vertical dashed lines in Figure 4.1.2.1 represent the ticks of a clock. UPS, as the name implies, is a pulse train of equal spacing, where pulses occur at the clock ticks. OOK refers to the process of selectively "turning off" or eliminating pulses at the clock ticks. ARD produces pulses that are dithered in relation to the clock tick. RRD dithers each pulse in relation to the previous pulse position.

The PRF for UPS, OOK, and ARD is equal to the clock rate; for our purposes, the PRF of RRD is defined as the reciprocal of the mean pulse interval. The extent of dither is expressed in terms of the percentage of pulse repetition period, which is the reciprocal of PRF.

Gating refers to the process of distributing pulses in bursts. This is represented in Figure 4.1.2.1 by the removal of the pulses in the shaded areas; in the case of the UPS example, there are 4 pulses generated during the gated-on time followed by 8 clock ticks for which there are no pulses (to give a duty cycle of 33%).

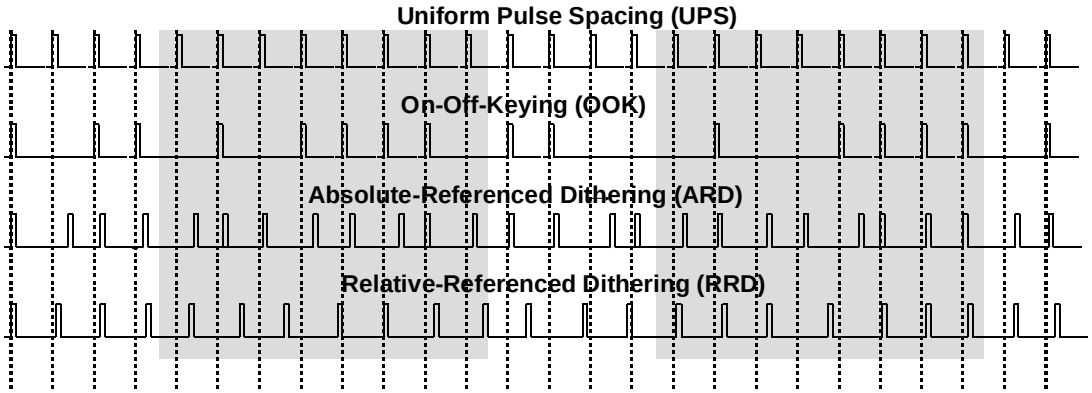

Figure 4.1.2.1. Pulse spacing modes.

UWB Signal Space

By varying the three parameters – PRF, pulse spacing, and gating – 32 different permutations were chosen to span the full range of existing and potential UWB signals. For these measurements (as shown in Table 4.1.2.1) there are four PRFs (i.e., 0.1, 1, 5, and 20 MHz), four pulse spacing modes (i.e., UPS, OOK, 50% ARD, and 2% RRD), and two

gating scenarios (i.e., no gating and 20% gating with a 4 ms on-time). In addition, various combinations of UWB signals were summed to produce aggregate signals as shown in Table 4.1.2.2.

Table 4.1.2.1. UWB Signal Space

UWB Signal Parameter	Range
Average Power Density	As needed to induce effect on GPS receiver.
Pulse Width	0.245 and 0.5 nanoseconds
Pulse Repetition Frequency	0.1, 1, 5, 20 MHz
Modulation, Dithering	UPS, OOK, 50%-ARD, 2%-RRD
Gating	100% (no gating) and 20% Duty Cycle

Table 4.1.2.2. Aggregate UWB Signal Space

Aggregate	UWB Signal Parameters
1	6 × 10-MHz PRF, 2%-RRD, Non-Gated
2	6 × 10-MHz PRF, 2%-RRD, Gated (20% Duty Cycle)
3	2 × 10-MHz PRF, UPS, Non-Gated 1 × 3-MHz PRF, UPS, Non-Gated 3 × 3-MHz PRF, 2%-RRD, Gated (20% Duty Cycle)
4	3 × 3-MHz PRF, UPS, Gated (20% Duty Cycle) 3 × 3-MHz PRF, 2%-RRD, Gated (20% Duty Cycle)
5	(a) 1 × 1-MHz PRF, 2%-RRD, Non-Gated (b) 2 × 1-MHz PRF, 2%-RRD, Non-Gated (c) 3 × 1-MHz PRF, 2%-RRD, Non-Gated (d) 4 × 1-MHz PRF, 2%-RRD, Non-Gated (e) 5 × 1-MHz PRF, 2%-RRD, Non-Gated (f) 6 × 1-MHz PRF, 2%-RRD, Non-Gated

Spectral Considerations

Spectral plots are shown in Figure 4.1.2.2 for four different UWB signals as they are passed through an L1 bandpass filter. UPS has the power gathered up into spectral lines at intervals of PRF. The greater the PRF, the wider the line spacing, and the greater the power contained in each spectral line. OOK also has spectral lines spaced at intervals of PRF that are superimposed on continuous noise-like spectrum. Dithered signals have spectral

characteristics inherently different from either UPS or OOK. For these measurements, ARD has a pulse spacing that is varied by 50% of the referenced clock period. RRD has a pulse spacing that is varied by 2% of the average pulse period. Both of these dithered cases have spectral features that are characteristic of noise (i.e., no spectral lines).

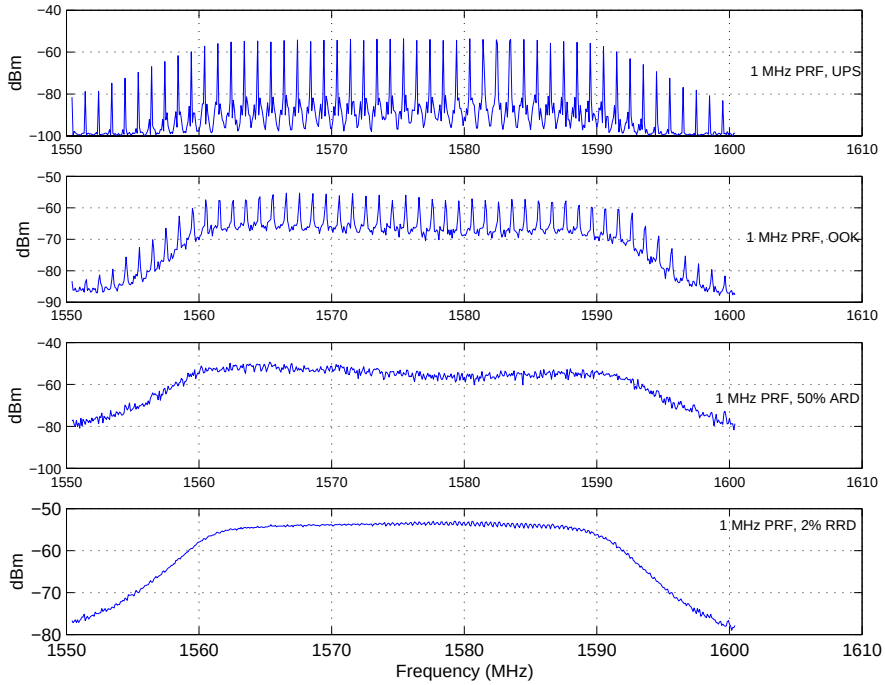

Figure 4.1.2.2. Spectral characteristics of the different pulse spacing modes.

Another feature worth noting is the phenomenon of spectral lines spreading due to gating. The spectrum of the gated UWB signal is the result of convolving the non-gated spectrum with the Fourier transform of the gating signal, which for our purposes is a sinc^2 envelope. It follows that the single line of the non-gated cases is spread out into a multitude of lines confined by the sinc^2 envelope, where the spacing between lines, or line spread spacing (LSS), is equal to the reciprocal of the gating period; null spacing, or line spreading null-to-null bandwidth (LSNB), of the main lobe of the sinc^2 function is equal to two times the reciprocal of gated-on time.

There are two additional spectral features that occur as a result of the signals having been generated by an arbitrary waveform generator (AWG). One is related to how the pattern of pulses is repeated, and the other has to do with the process of placing the pulses into bins, representing discrete dithered pulse spacing. Further discussion of these spectral characteristics of UWB signals is contained in Appendix C.

Spectral Line Alignment

Because each of the emulated satellites is mobile in nature, there is a corresponding Doppler shift associated with its motion and direction. Figure 4.1.2.3 shows the emulated Doppler frequency for SV 25 going from the beginning to the end of the simulation. Notice that the C/A code lines shift nearly 2.25 kHz over the course of the simulation. For those UWB signals which contain spectral lines, alignment of the UWB spectral lines and the SV-25 spectral lines over a period of 40 minutes is inevitable. To assure controlled measurement conditions, both the GPS simulator and the AWG were time referenced with the same rubidium oscillator and the spectral lines of the UWB signals were precisely placed, as described in detail in Appendix C, Table C.1.1. Figure 4.1.2.4 illustrates the manner in which these spectral lines were placed. Because SV 25 has a particularly vulnerable spectral line at 1575.571000 MHz, each of the UWB signals with discrete spectral lines were created with a spectral line at 1575.570571 MHz – approximately half way between GPS spectral lines. As described in Section 4.3, data acquisition started at 20 minutes into the simulation (at approximately 0 Hz Doppler shift) and continued for the next 20 minutes; hence, spectral alignment was guaranteed.

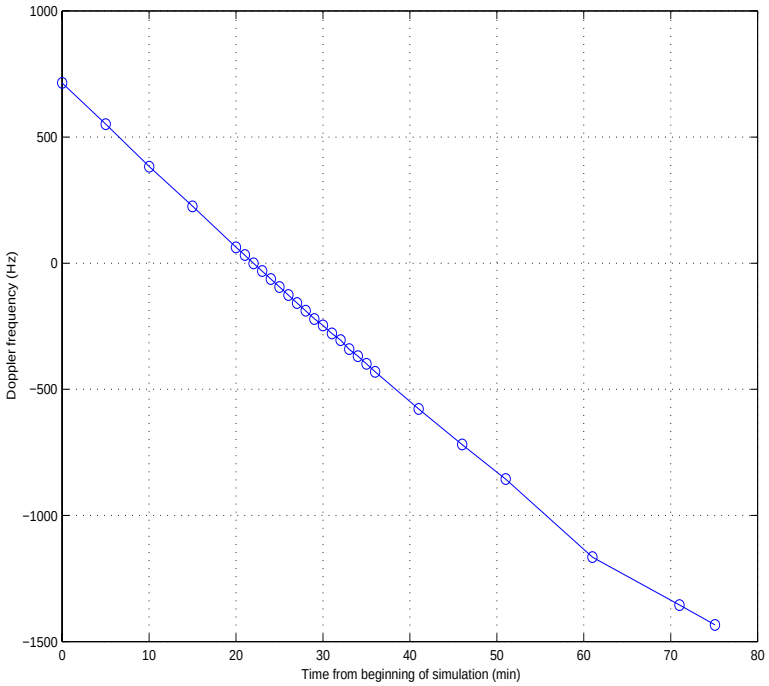

Figure 4.1.2.3. Doppler frequency of SV25.

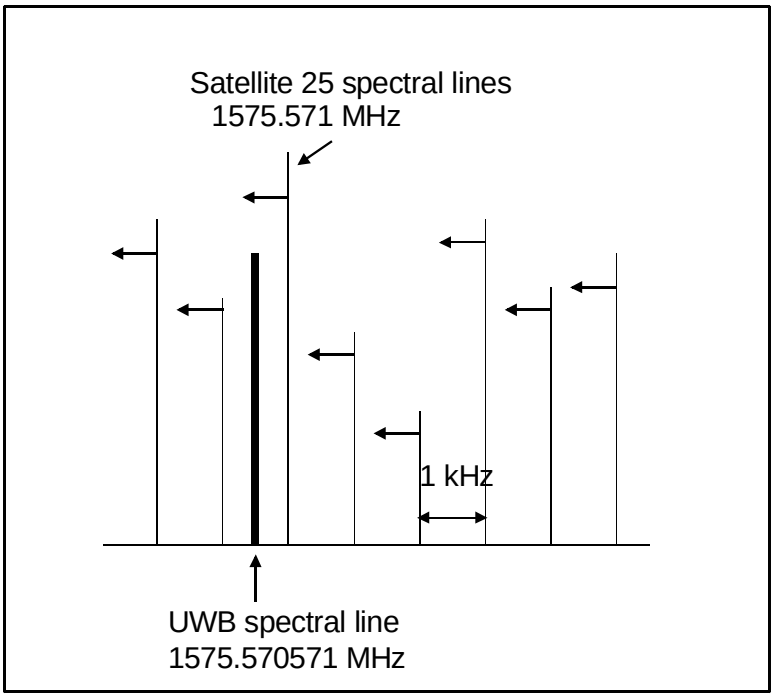

Figure 4.1.2.4. Spectral line placement.

4.1.3 GPS-Receiver Segment

The typical stand-alone GPS receiver is implemented on specialized ASICs and DSP chips. The information from GPS signals is processed, according to proprietary adaptive algorithms, to meet design specifications for specific applications. For example, navigational receivers require reliable position information and fast recovery from outages, while surveying receivers require high-precision position accuracy. Each receiver may generate different failure modes from interference and may recover from interference in different ways.

Two receivers encompassing different technologies were selected and are given in Table 4.1.1. These receivers employ various techniques to accomplish their individual design specifications. As a rule of thumb, the receivers under test were left at their factory default settings with two exceptions. First, stand-alone mode was always specified; that is, DGPS, pseudolites, and external sensors (e.g., altimeters, inertial navigation equipment) were disabled. Secondly, carrier smoothing was removed whenever possible in order to minimize the number of correlated data points. Appendix B provides a table of settings for each receiver.

Each receiver has an active antenna with a specific gain and bandwidth. Because the conducted measurements bypassed the antenna, input signals were filtered and amplified to give an equivalent bandwidth and gain of the respective receiver antenna. A preselection filter and low noise amplifier (LNA) were placed in front of the receiver for the purpose of

matching, as close as possible, the filter and amplifier characteristics of the antenna unit. Receiver 2, however, required an active L1/L2 filter with a 27-MHz bandwidth which is approximately half the bandwidth of the accompanying antenna.

It is assumed that the receiver bandwidth sets the narrowest bandwidth for signal path, and therefore, the equivalent antenna bandwidth filter is not critical to the outcome of the results. This was verified by measurements using two different equivalent antenna bandwidths for the same receiver. However, for practical purposes, the preselector filters were also used to prevent saturation of amplifiers utilized in the test fixture. The discussion on radiated versus conducted measurements, given in Appendix A, is also relevant to this topic.

4.2 Power Measures, Settings, and Calibration

The purpose of this section is to clarify power measurement terminology, discuss power level settings of the various signal sources, and describe the calibration procedures used to assure the proper power levels.

4.2.1 Carrier-to-Noise Density Ratio Settings

To account for other potential sources of interference, such as sky noise, cross-correlation noise from other satellites within the GPS constellation, and GPS augmentation systems, broadband noise was added to the GPS-source segment. The level of broadband noise – based on minimum C/N_0 requirement for acquisition of a GPS satellite – was set to 34 dB-Hz [3]. Based on the minimum guaranteed GPS signal power (C) specification for the C/A code of -130 dBm into a 0 dBic gain antenna [4] and a 2 dB implementation loss (L_{imp})[1] the maximum broadband noise density level at which satellite acquisition can be ensured is:

$$N_0 = C - L_{imp} - C/N_0 = -130 - 2 - 34 = -166 \text{ dBm/Hz}.$$

Because the broadband noise was measured at the output of a 20-MHz bandpass filter, the added-noise power level is then calculated as:

$$N = -166 + 10 \log (20 \times 10^6) = -93 \text{ dBm/20 MHz}.$$

The use of a broadband noise level based upon the C/N_0 acquisition threshold is supported by computer simulations performed within the International Telecommunication Union Radiocommunications Sector (ITU-R). The simulations in ITU-R Recommendation M.1477 show how C/N_0 can vary over a 24-hour period, at different user locations, when only sky

[1] The implementation loss takes into account the loss due to IF filtering, the loss due to the analog-to-digital conversion, correlation loss due to modulation imperfections in the GPS signal and other miscellaneous losses.

noise and GPS cross-correlation noise are considered. The results of this simulation indicate that without any additional interference from external sources, and under certain worst case conditions, the C/N_0 level can fluctuate to within 1 dB of the acquisition threshold of 34 dB-Hz.

4.2.2 Calibration and Power Level Correction

For these measurements, all signal powers were measured with a power meter and expressed as a mean value. Wideband sources, such as UWB signals and noise, are expressed in terms of power density in a 20-MHz bandwidth (centered at 1575.42 MHz). This section describes the various steps taken to assure power-level accuracy.

To assure that no test-fixture amplifier became saturated throughout the measurements and verify functionality, power levels were measured throughout the test fixture using the full range of signals and power levels. Amplifiers, in addition, were tested for linearity – also using the full range of signals and power levels.

Prior to every interference measurement, power levels of the GPS, noise, and UWB signals were measured without attenuation imposed. Measured power at TP4 and TP6 (in Figure 4.1.2) are referenced to the input of the LNA (TP7) via calibration factors which account for the losses associated with individual power-measurement paths. During the test, contributing power levels were determined by subtracting an applied attenuation from the respective 0-dB attenuation measurements. Additionally, each attenuator was checked for integrity before each test.

Because noise was measured in a bandpass filter centered at the L1 frequency, and because some power passed through the filter outside the 20-MHz bandwidth, a power correction was applied. This correction factor was determined by passing the noise through the filter and measuring the noise power with a spectrum analyzer over a range of frequencies centered at 1575.42 MHz. The power was integrated over 100 MHz and then integrated again across 20 MHz. The difference between these two values (in dB) is subtracted from the measured noise power, giving a spectral power density in the 20 MHz bandwidth.

To assure proper and consistent power levels at the output of the GPS simulator, the GPS signal power of SV 25 was measured at the beginning of each test. All other satellites were turned off during power measurement. To reduce the noise contribution and exclude the L2 signal, the power was measured through an L1 bandpass filter centered at 1575.42 MHz; however, because the power meter measures both the C/A and P code, a calibration factor was applied to determine the power of the C/A code only. This calibration factor was determined by measuring and theoretically verifying the difference in power levels between having only the C/A code turned on and having both the P and C/A codes turned on.

Two other issues regarding power settings has to do with measuring and setting the power of gated and aggregate signals. Because the power meter does not accurately measure gated signal powers, all gated signal powers were measured without gating. As mentioned earlier, the power of all gated signals, used during interference measurements, is expressed as the average power of the non-gated signal. Twenty percent gating reduces mean non-gated signal power by 7 dB. Finally, all signals contributing to the aggregate signals shown in Table 4.1.2.2 have equal peak powers.

4.3 Measurement Procedure

In this experiment, two separate tests were performed to measure break-lock and reacquisition-time behavior (flowcharts are given in Figures 4.3.1 and 4.3.2, respectively). The procedures were implemented in software to enhance repeatability, automate testing, and provide a vehicle for extracting information from the receivers.

During RQT measurements, the GPS simulator used a dynamic scenario emulating a mobile receiver traveling at 10 m/s. During BL measurements, a static scenario was used. The measurements were delayed 20 minutes every time the simulator was reset. This twenty-minute delay is based on the fact that it takes a minimum of 12.5 minutes for the receiver to download the entire navigation message from the constellation; hence, we assume 20 minutes is enough time for the almanac/ephemeris data inside the receiver to be up-to-date and complete.

The basic BL measurement consists of turning off interference, reestablishing lock, turning on interference, and sampling the receiver's loss-of-lock indicator once per second over the BL measurement duration (approximately 17 minutes). The BL test shown in Figure 4.3.1 determines the BL point. This is accomplished by incrementing UWB signal power by 3 dB between BL measurements until BL occurs. The BL test then decrements the UWB signal power in 1-dB steps until lock is maintained continuously over the entire measurement duration. The BL point is defined as 1 dB above this final UWB signal power. During BL measurements, the following observational parameters were sampled once per second for data analysis: pseudorange, observation time, clock offset, carrier phase, Doppler frequency shift, signal-to-noise ratio, potential cycle slip, position data, and receiver tracking status.

The basic RQT measurement consists of turning off the zenith satellite, setting the interference level, delaying 10 seconds, turning on the zenith satellite, applying the interference, and measuring the number of seconds until the receiver achieves lock. A RQT measurement is successful if lock is achieved within 2 minutes and maintained for at least 1 minute. The RQT test summarized by the flowchart in Figure 4.3.2 is performed by incrementing UWB signal power by 3 dB between sets of 10 RQT measurements. The test is complete when all 10 RQT measurements at a single UWB power are unsuccessful.

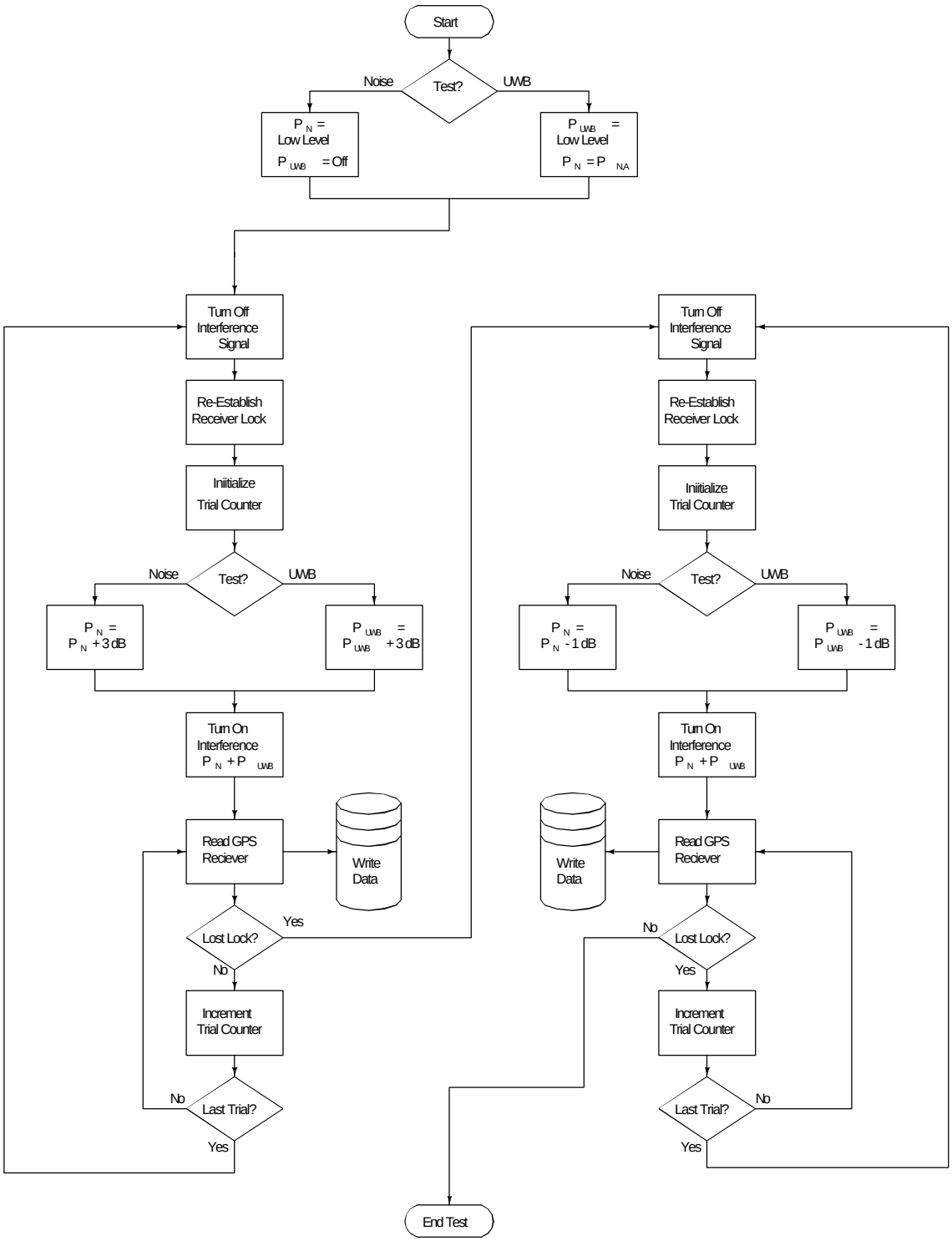

Figure 4.3.1. Break-lock test flowchart.

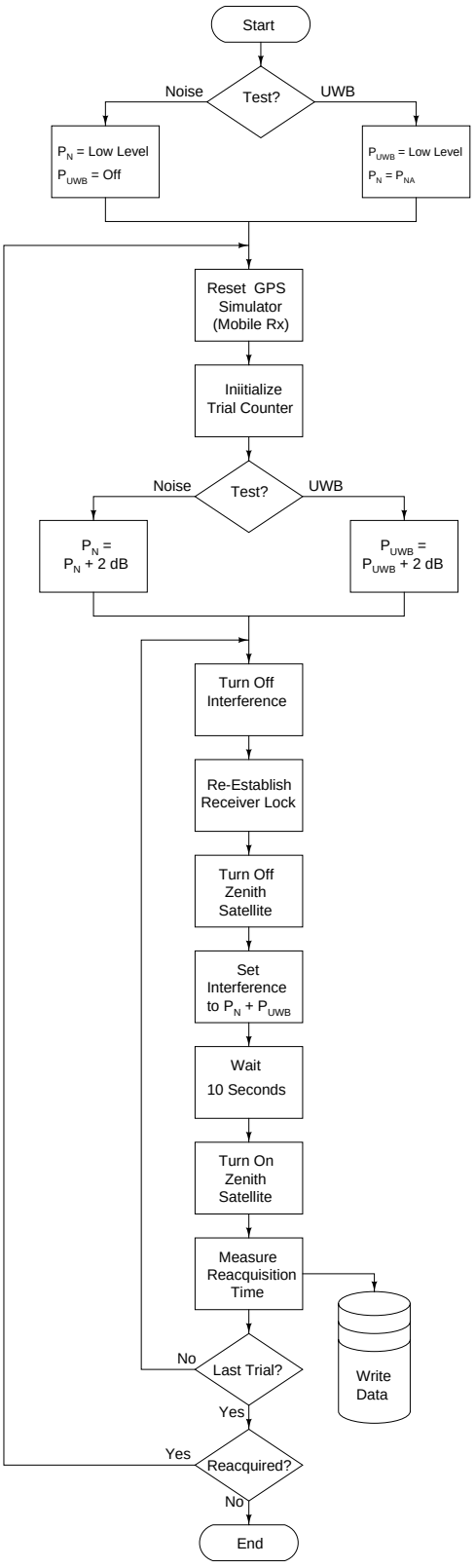

Figure 4.3.2. RQT test flowchart.

5. DATA ANALYSIS

Data analysis consists of characterizing the UWB interference and quantifying the effects of the interference on GPS receiver signal acquisition, signal tracking, and range estimation functions. The effects of UWB interference on signal acquisition and signal tracking are characterized with the BL point and RQT operational metrics. The effects of UWB interference on range estimation are characterized with observational metrics such as the statistics of range error.

5.1 UWB Signal Characterization

Band-limited UWB signals can be decomposed into time-varying amplitude and phase functions. Engineers, in the past, have found strong correlation between signal amplitude statistical characteristics and receiver performance. Therefore it should not be surprising that signal amplitude statistical characteristics are suspected as being correlated to GPS receiver performance degradation.

Signal amplitude statistics are often visualized with the APD. The APD shows the probability or percent of time a signal will exceed an amplitude value. Formally:

$$F_A(a) = P(A>a) \quad ,$$

where A is the amplitude random variable and a is an amplitude value. The APD is the compliment of the amplitude cumulative distribution function (CDF) which describes the probability a signal amplitude will be less than or equal to an amplitude value. The APD can also be written in terms of the CDF as:

$$F_A(a) = 1 - P(A \le a) \quad .$$

APDs are often plotted on a Rayleigh graph where the amplitude of Gaussian noise is represented by a negatively sloped, straight line. Gaussian noise mean power corresponds to the power at the 37th percentile.

Non-Gaussian signals have APDs that deviate from the straight line when plotted on a Rayleigh graph. Non-Gaussian signal mean power cannot be read directly from the APD. However, when the power samples are normalized by some reference power, power ratios (peak-to-mean or peak-to-median) can be determined. In addition, the percentage of time a non-Gaussian signal is present can be read from the APD.

The “Gaussian-ness” of the band-limited UWB signal is dependent on the signal pulse repetition frequency and pulse-spacing specifications and the bandwidth of the receiver filter. Figure 5.1.1 shows two UWB signal APDs along with a Gaussian noise APD. The curves are normalized to 0-dBm/20MHz mean power. The first APD corresponds to a UWB signal with a 1-MHz PRF and uniform pulse spacing. The second APD corresponds to a UWB signal with a 1-MHz PRF and 2% relative referenced dithering. Because the PRF is much less than the bandwidth, the pulses are resolved, and the amplitude statistics are nearly identical. Therefore, the two curves lie on top of each other. Both have approximately 10 dB peak to mean power ratios. The pulse is present approximately 60% of the time.

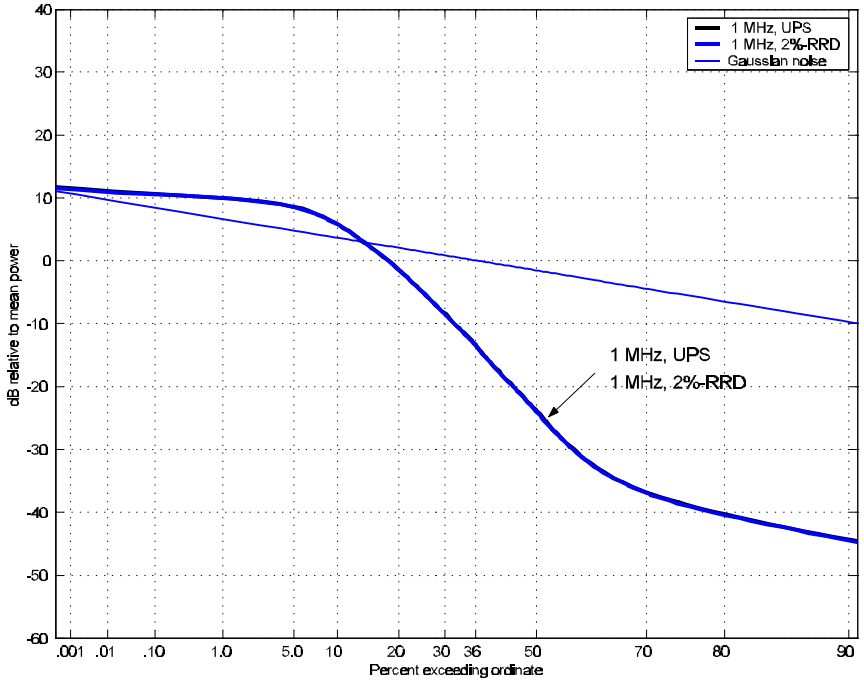

Figure 5.1.1 APDs for Gaussian noise, 1-MHz PRF with UPS, and 1-MH PRF with 2% RRD.

A complete collection of APDs derived from samples of UWB interferers used during BL and RQT tests can be found in Appendix C. These APDs were acquired with 3 MHz and 20 MHz bandwidths. A detailed tutorial on the APD can be found in Appendix E.

5.2 Operational Metrics

5.2.1 Break-lock Point

The BL point is the UWB signal power level that causes a receiver in tracking mode to re-enter acquisition mode. For some receivers, BL refers to the failure of C/A code delay tracking while for other receivers, BL refers to loss of carrier phase tracking.

Theoretically BL is a binomially distributed random process - the receiver is either locked or not. Thus BL can occur over a range of UWB signal levels and is likely to vary with BL measurement duration. Rather than assigning a BL point, it would be more accurate to assign a BL probability to every UWB signal level tested. Unfortunately, repeated BL measurements at various power levels and BL measurement durations are not practical.

Thus, for analysis purposes, the BL point is defined to be 1 dB above the maximum UWB signal power, where the receiver is able to maintain lock during the entire BL measurement duration, while the BL test is decrementing. At times, the receiver was able to maintain lock at a UWB signal power when the BL test was incrementing but lost lock at the same level while the BL test was decrementing. In this case the BL point is defined to be 1 dB above this UWB signal power.

5.2.2 Reacquisition Time

The RQT is the time it takes a receiver, forced from tracking to acquisition by the sudden removal of the satellite signal, to reenter tracking mode. As in BL, for some receivers tracking refers to the C/A code delay tracking, while for other receivers it refers to the carrier phase tracking.

RQT is assumed to be a Gaussian distributed random variable. However; no test was formally conducted to confirm this. Furthermore, there is a binomially distributed element to the RQT test since RQT measurements are not always successful. A RQT measurement is unsuccessful when reacquisition is not obtained in less than RQT_{max} seconds. When the measurement is unsuccessful , in principle, no RQT exists.

Rather than ignore the unsuccessful measurement a new random variable was defined:

$$6 = \min(RQT, RQT_{max}) \ .$$

The mean 6 was then used for analysis purposes:

$$m_{\kappa} = \frac{1}{N} \sum_{n=1}^{N} \kappa_n \quad ,$$

where *N* is the number of RQT measurements.

If all measurements are successful, then mean 6 is equivalent to the mean RQT. This is no longer true if at least one measurement is unsuccessful. The advantage of using mean 6 is that it steadily converges to RQT_{max} with increasing UWB signal level. In contrast, mean RQT becomes more variable due to the decrease in the number of successful measurements.

5.3 Observational Metrics

Range, cycle slip, and SNR observational metrics were derived from data acquired during the BL measurement. Cycle slip and SNR require minimal additional processing. However, range requires a considerable amount of processing to yield useful analysis information.

5.3.1 Range Performance

Degradation of the range estimate is determined by analysis of range error statistics. Range error values were derived from subtracting a known, simulated range from the range measured by the GPS receiver. The range error statistic was found to be time dependant and therefore non-stationary. This non-stationarity was introduced by systematic errors due to the GPS radio environment and spectral line interference. A calibration and correction procedure was developed to remove the systematic component, giving a range error residual – the statistics of which were then used for analysis.

Range

Two range estimates – pseudorange (PSR) and accumulated delta-range (ADR) – were derived from observables sampled during the BL measurement. PSR is the most fundamental range measurement derived from correlation of the C/A code. The prefix *pseudo* highlights the fact that satellite and receiver clocks are not synchronized. ADR is an ambiguous range corresponding to the accumulated differences in range from one time to another. ADR is derived from observation of the Doppler-shifted radio frequency carrier. Although the ADR is ambiguous, it has much less uncertainty than PSR. This ambiguity can be resolved with a time-averaged code-minus-carrier (CMC) range bias which is defined to be the difference between the PSR and ADR.

Fundamentally, PSR (m) is defined by

$$\rho = c(t_u - t_s) \quad ,$$

where c is the speed of propagation (m/s), t_u is the received time (s), and t_s is the transmitted time. An alternative expression for PSR is

$$\rho(t) = |\boldsymbol{r}_s(t) - \boldsymbol{r}_u(t)| + \epsilon_\rho(t) \quad ,$$

where bold letters represent vectors, $\boldsymbol{r}_s$ is the position of the satellite, $\boldsymbol{r}_u$ is the position of the user receiver, $|\boldsymbol{r}_s - \boldsymbol{r}_u|$ is the geometric range between the two positions, and ϵ_D is the PSR error (m).

ADR is derived from the delta-PSR (DPSR) velocity measurement. The DPSR is defined by the rate of change of PSR (m/s)

$$\delta(t) = [\boldsymbol{v}_s(t) - \boldsymbol{v}_u(t)] \cdot \boldsymbol{1}(t) + \epsilon_\delta(t) \quad ,$$

where $\boldsymbol{v}_s$ is the velocity of the satellite (m/s), $\boldsymbol{v}_u$ is the velocity of the receiver, ϵ_* is the DPSR error, and $\boldsymbol{1}$ is the unit range vector between the satellite and the receiver defined by

$$\boldsymbol{1}(t) = \frac{\boldsymbol{r}_s(t) - \boldsymbol{r}_u(t)}{|\boldsymbol{r}_s(t) - \boldsymbol{r}_u(t)|} \quad .$$

DPSR can also be expressed as a function of Doppler frequency shift D (Hz) since

$$\lambda D(t) = [\boldsymbol{v}_s(t) - \boldsymbol{v}_u(t)] \cdot \boldsymbol{1}(t) \quad ,$$

where λ is the carrier frequency wavelength (m). Substitution gives

$$\delta(t) = \lambda D(t) + \epsilon_\delta(t) \quad .$$

Integrating DPSR yields ADR formally defined as

$$\alpha(t_1, t) = \int_{t_1}^{t} \delta(\tau)\, d\tau = |\boldsymbol{r}_s(t) - \boldsymbol{r}_u(t)| + \epsilon_\alpha(t) \quad ,$$

where t_1 is the integration starting time and ADR error is related to DPSR error via

$$\epsilon_\alpha(t_1, t) = \int_{t_1}^{t} \epsilon_\delta(\tau)\, d\tau \quad ,$$

Finally, CMC is formally defined as

$$\chi(t_1, t) = \rho(t) - \alpha(t_1, t) \quad .$$

CMC minimizes systematic errors common to both PSR and ADR and helps isolate the effects of interference.

Examples of simulated PSR, DPSR, ADR, and CMC are shown in Figure 5.3.1.1. These parameters are taken from the simulator "log" file which provides true range data used to calculate range error in the next section. Simulation time is the time from the start of the simulation. PSR is from approximately 20.4×10^6 m to 20.8×10^6 m. The satellite is at zenith when the PSR is a minimum at approximately 1300 s. DPSR is a relatively straight line with negative velocities as the satellite approaches and positive velocities as it recedes. The DPSR is 0 m/s at zenith corresponding to a 0-Hz Doppler shift. ADR is 0 m at the start of the simulation. The ADR decreases as the satellite approaches and increases as the satellite recedes. The ADR curve is similar to the PSR curve without the initial range offset. CMC is constant at this offset from start to finish.

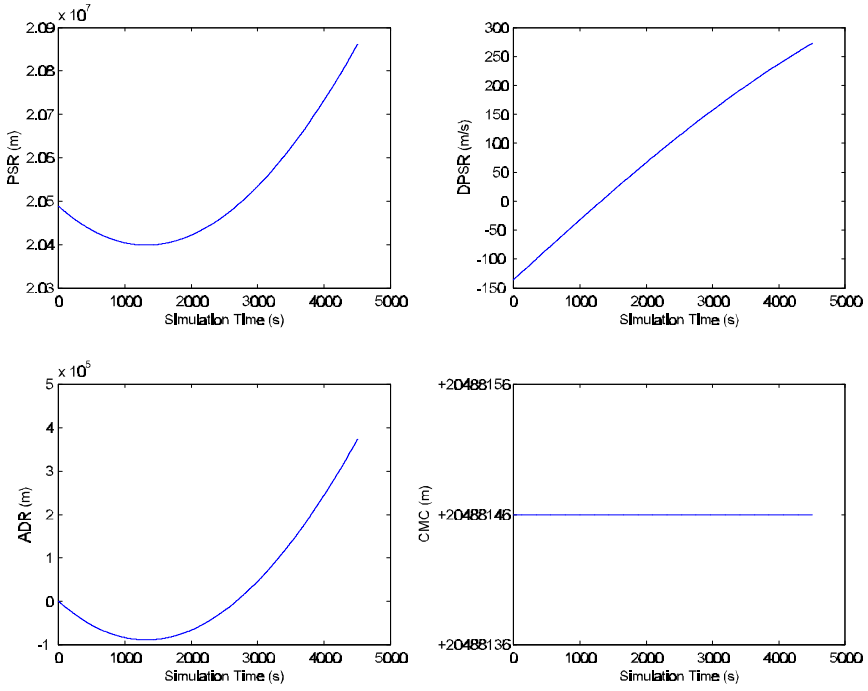

Figure 5.3.1.1 Simulated values.

Range Error

Measured ranges have more sources of error than simulated ranges [5, 6]. For example, measured PSR is represented by

$$\hat{\rho}(t) = |\boldsymbol{r}_s(t) - \boldsymbol{r}_u(t)| + c\hat{b}_u(t) + \hat{\epsilon}_\rho(t) \quad ,$$

where $\hat{}$ denotes measured values and b_u is the receiver clock offset (s). This expression demonstrates that measured ranges are influenced by receiver noise and clock inaccuracies. These error sources are also present in DPSR as expressed by

$$\hat{\dot{\rho}}(t) = \lambda\hat{D}(t) + c\frac{d\hat{b}_u(t)}{dt} + \hat{\epsilon}_\delta(t) \quad ,$$

and consequently ADR. Computation of ADR alone sometimes requires compensation of the clock offset for Doppler effects. Computation of ADR for CMC does not require this compensation because these effects are also present in PSR.

Examples of measured PSR, DPSR, ADR, and CMC are shown in Figure 5.3.1.2. These parameters were measured using Rx 1 with -93 dBm/20MHz Gaussian noise added to the GPS signal. The measured ranges are different from the simulated ranges in Figure 5.3.1.1. CMC shows measurement uncertainty most dramatically because systematic error was removed.

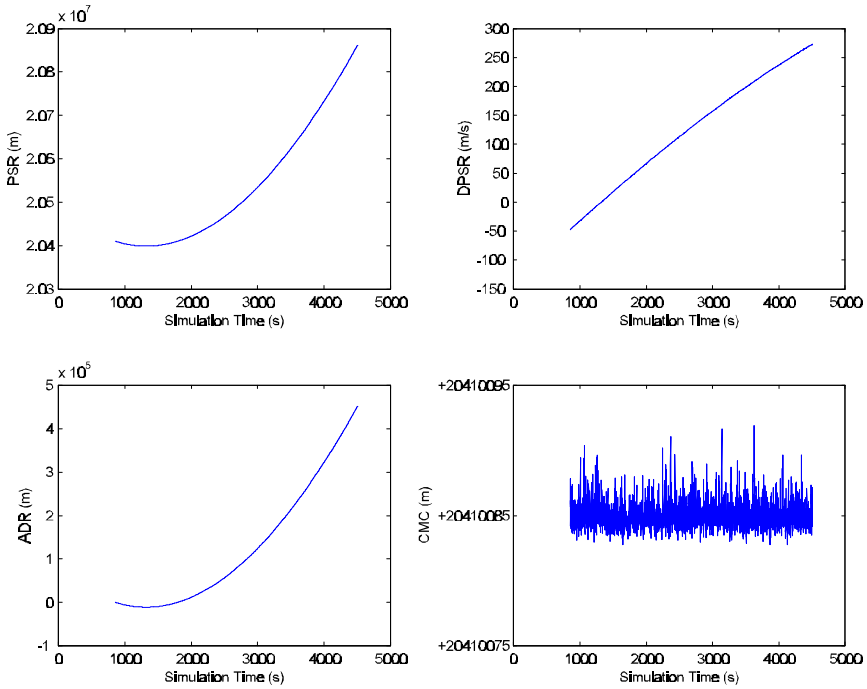

Figure 5.3.1.2 Reference measurement values.

Range error is the difference between simulated and measured range estimates. PSR error is

$$\Delta_\rho(t) = \hat{\rho}(t) - c\hat{b}_u(t) - \rho(t) = \hat{\epsilon}_\rho(t) - \epsilon_\rho(t) \quad ,$$

ADR error is

$$\Delta_\alpha(t_1,t) = \hat{\alpha}(t_1,t) - \alpha(t_1,t) = \hat{\epsilon}_\alpha(t_1,t) - \epsilon_\alpha(t_1,t) \quad ,$$

and CMC error is

$$\Delta_\chi(t_1,t) = \hat{\chi}(t_1,t) - \chi(t_1,t) = [\hat{\epsilon}_\rho(t) - \epsilon_\rho(t)] - [\hat{\epsilon}_\alpha(t_1,t) - \epsilon_\alpha(t_1,t)] \quad .$$

Figure 5.3.1.3 shows range error corresponding to the simulated and measured ranges in Figures 5.3.1.1 and 5.3.1.2. Notice that PSR and ADR cases have curved features while the CMC case is relatively flat. The curves are indicative of an underlying non-stationary process where the range-error statistic is dependent on time. This non-stationarity is undesirable and must be minimized before more detailed statistical analysis can proceed.

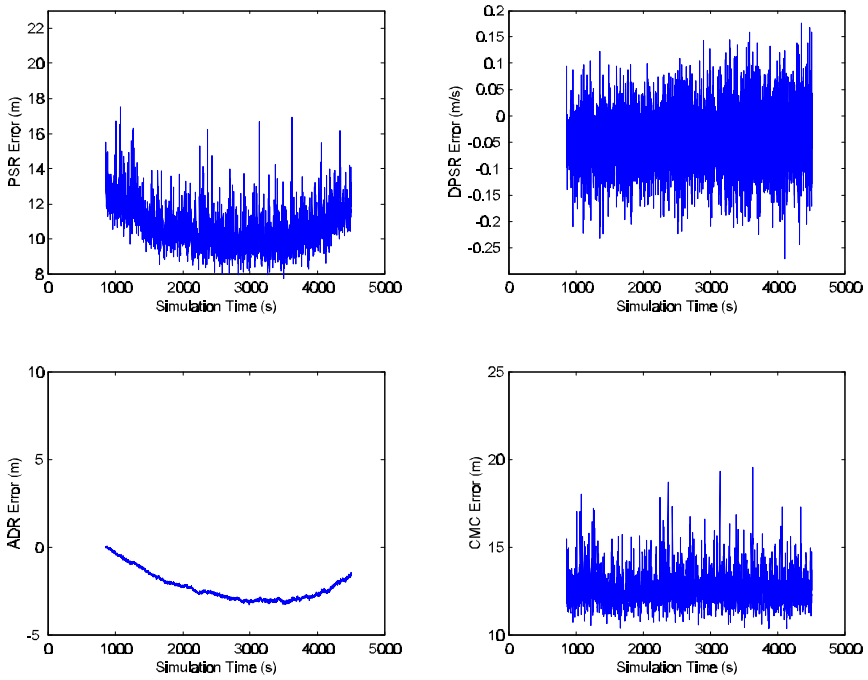

Figure 5.3.1.3 Reference range error.

Range error residual

In order to separate the effects of UWB interference, a general expression for range error is

$$\Delta = \Delta_{ref} + \hat{\epsilon}_{UWB} \quad ,$$

where the $)_{ref}$ is the reference range error and $\$_{UWB}$ is error introduced by UWB interference. We measure $)_{ref}$ under nominal SNR conditions specified in Table 4.1.1. Figures 5.3.1.2 and 5.3.1.3 show the reference range and reference range error for Rx 1, respectively.

The reference range error can be modeled as

$$\Delta_{ref} = \Phi_{ref} + \varphi_{ref} \quad ,$$

where M_{ref} represents the non-stationary systematic reference error and n_{ref} represents the random reference error and contains high-order components of $)_{ref}$. M_{ref} is a function derived from a 3rd order polynomial fit to $)_{ref}$. Figures 5.3.1.4 and 5.3.1.5 show these errors for Rx 1. Subtracting M_{ref} from $)_{ref}$ removes non-stationary systematic error and yields a range error residual

$$\gamma = \Delta - \Phi_{ref} = \hat{\epsilon}_{UWB} + \varphi_{ref} \quad ,$$

which is our best estimate to range error due to UWB interference.

Figures 5.3.1.6 and 5.3.1.7 show systematic along with measured range error for two different UWB interference signals. The first is 1-MHz PRF with UPS and no gating. The second is 1-MHz PRF with 2% RRD and no gating. In both cases, Rx 1 was exposed to the maximum UWB power levels where lock is maintained. The UPS case has spectral line interference starting at 2000 seconds. PSR, ADR, and CMC show significant changes in error at this point. Prior to this spectral alignment, the error coincides with M_{ref}. The 2% RRD case has an elevated range error when compared to M_{ref}.

Figures 5.3.1.8 and 5.3.1.9 show the range error residuals for these same UWB signals. Clearly the magnitude of the residuals is less. The increased error due to spectral line interference is still dominant in the UPS case.

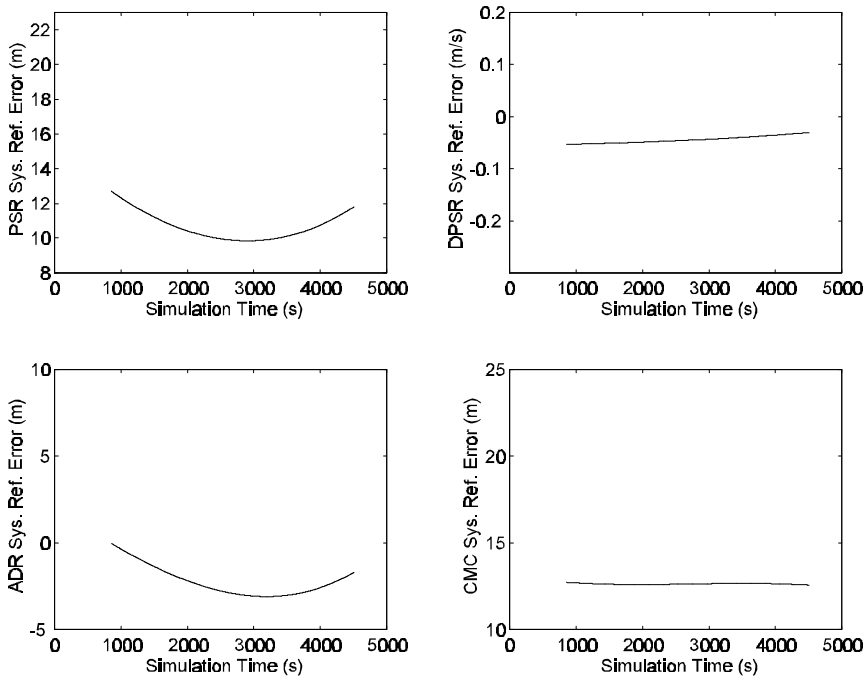

Figure 5.3.1.4 Systematic reference error (M_{ref}).

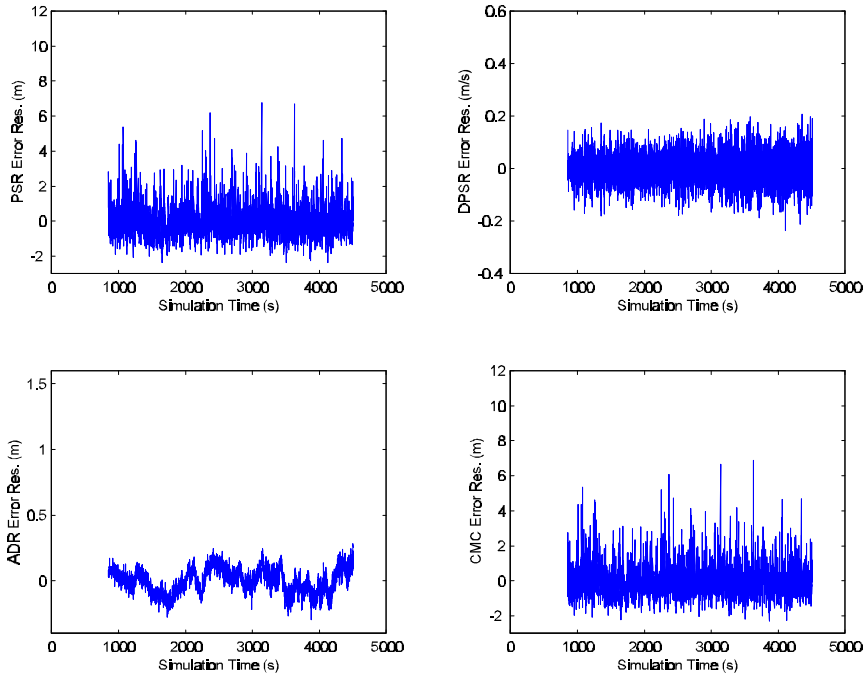

Figure 5.3.1.5 Random reference error (n_{ref}).

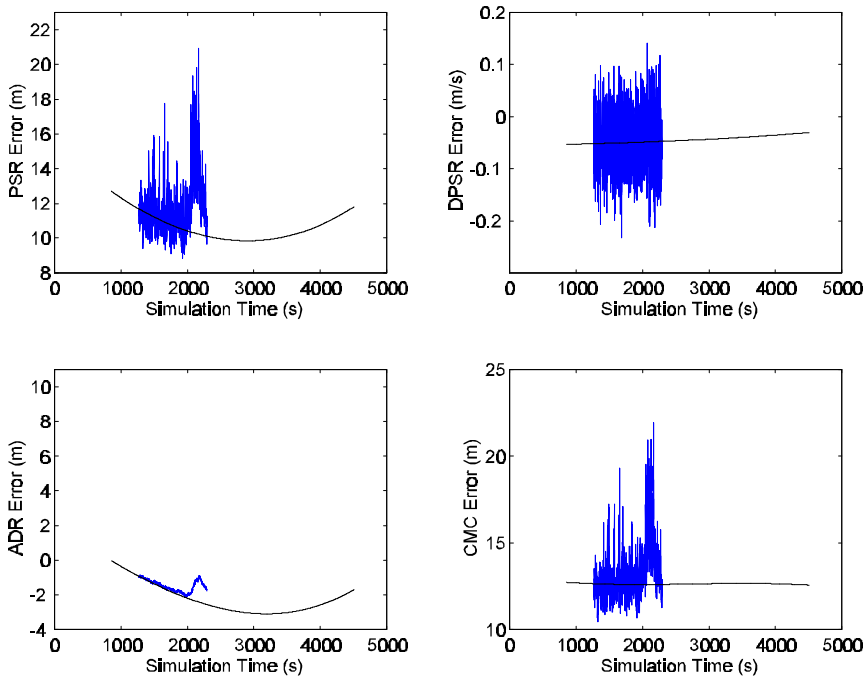

Figure 5.3.1.6 Range error due to 1-MHz PRF with UPS interference compared to systematic reference range error.

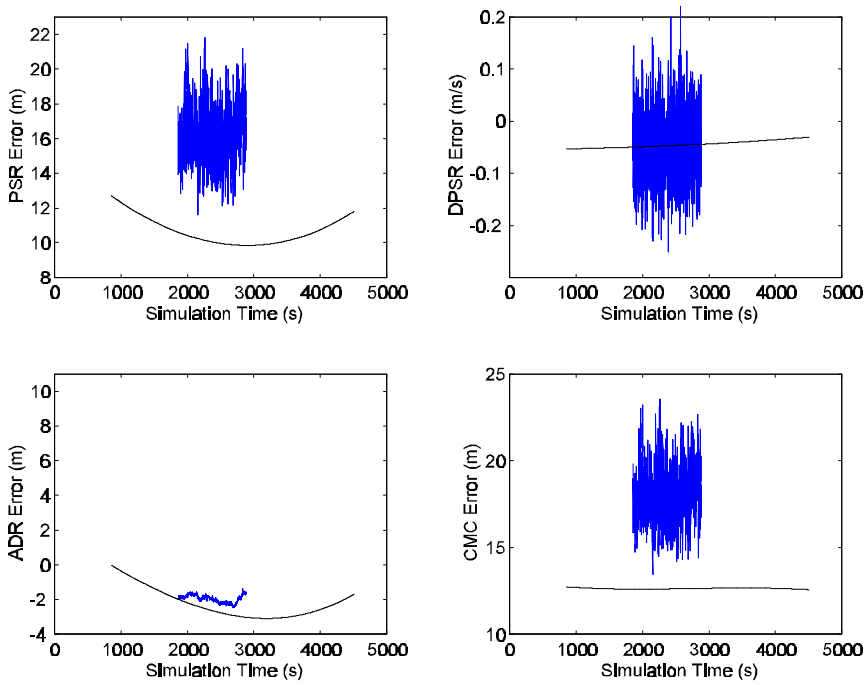

Figure 5.3.1.7 Range error due to 1-MHz PRF with 2%-RRD interference compared to systematic reference range error.

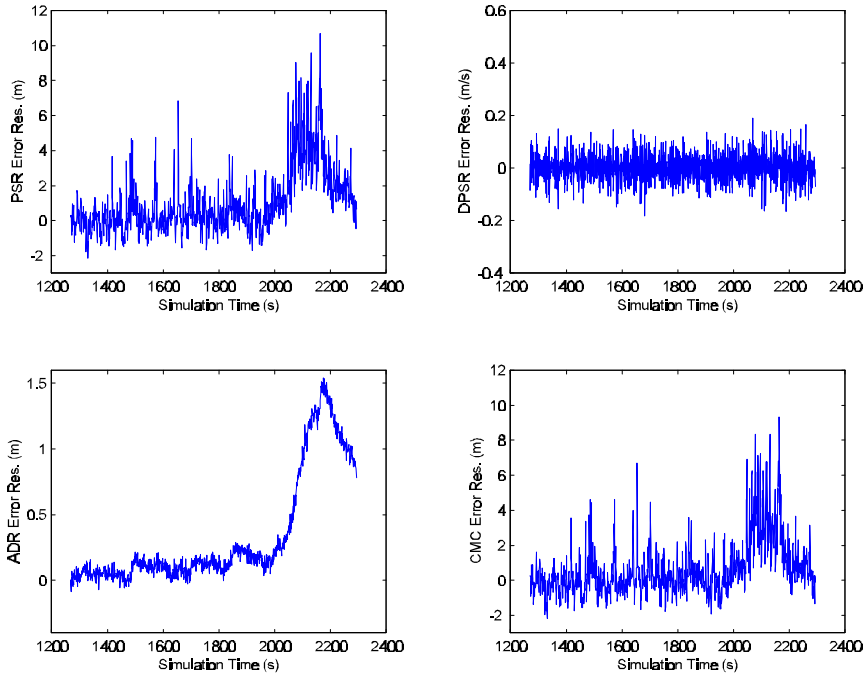

Figure 5.3.1.8 Range error residual due to 1-MHz PRF with UPS interference.

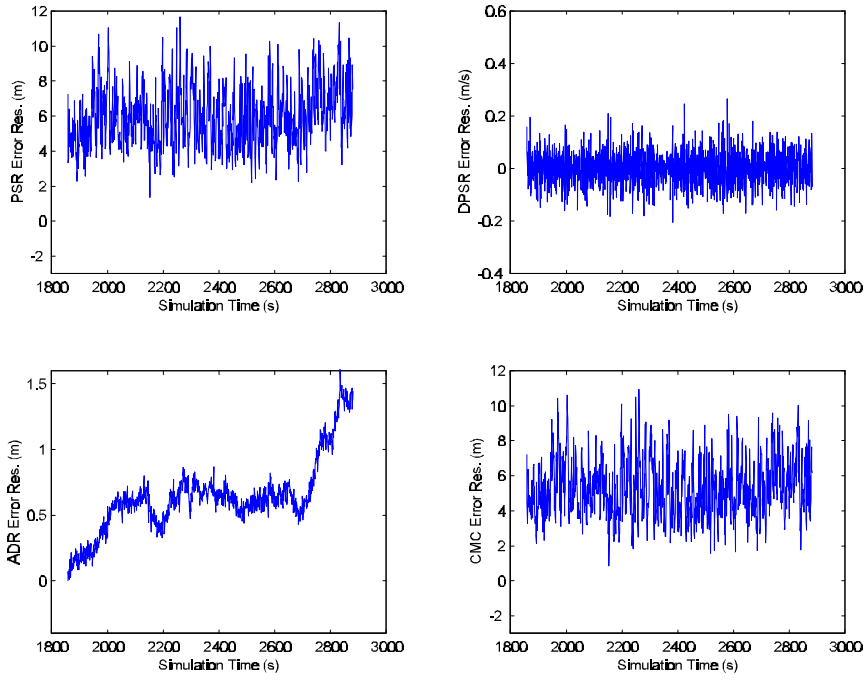

Figure 5.3.1.9 Range error residual due to 1-MHz PRF, 2%-RRD interference.

Range error residual statistics

The range error residual is analyzed with numerous statistics. Range error residual standard deviation is a commonly used statistic for evaluating the effect of interference. Zero-mean, Gaussian distributed random variables are completely described by the standard deviation statistic

$$\sigma_\gamma = \sqrt{\frac{1}{N}\sum_{n=1}^{N}(\gamma_n - m_\gamma)^2} \quad .$$

where *N* is the number of range error residual samples and *m* is the mean range error residual. Although this statistic was evaluated, it was deemed insufficient because the range error residuals were often non-Gaussian. Therefore, in addition to standard deviation, other statistics including percentiles were analyzed [7].

Percentiles are computed from the CDF defined by

$$F_\Gamma(\gamma) = P(\Gamma \le \gamma) \quad ,$$

where ' is the range error residual random variable. The CDF is most easily obtained by sorting the sampled (into ascending values. The probability corresponds to the position in the sorted array. The median, 84th, and 98th percentiles represent the range error residual value that are greater than or equal to all others 50, 84, and 98% of the time. The 84th and 98th percentiles are significant because they represent the 1 and 2 standard deviation values for a zero-mean Gaussian distributed random variable.

Figures 5.3.1.10, 5.3.1.11, and 5.3.1.12 show the range error residual CDFs of the reference measurement and the two 1-MHz PRF cases described above. These CDFs are plotted on a Gaussian graph where a Gaussian distributed random variable is represented by a positively sloped, straight line. The UPS case deviates from this line at approximately the 84th percentile. This percentile corresponds to the time the spectral line interference is present during the BL measurement. The CDF of the 2% RRD case appears Gaussian. The percentiles for PSR and CMC track each other in both cases. This is to be expected since CMC error is dominated by PSR error.

The skewness, excess, and median-to-mean ratio statistics quantify the “Gaussian-ness” of the range error residual. The skewness measures the symmetry of a probability density function and is defined by

$$\beta_1 = \frac{1}{\sigma^3}\sqrt{\frac{1}{N}\sum_{n=1}^{N}(\gamma_n - m_\gamma)^3} \quad .$$

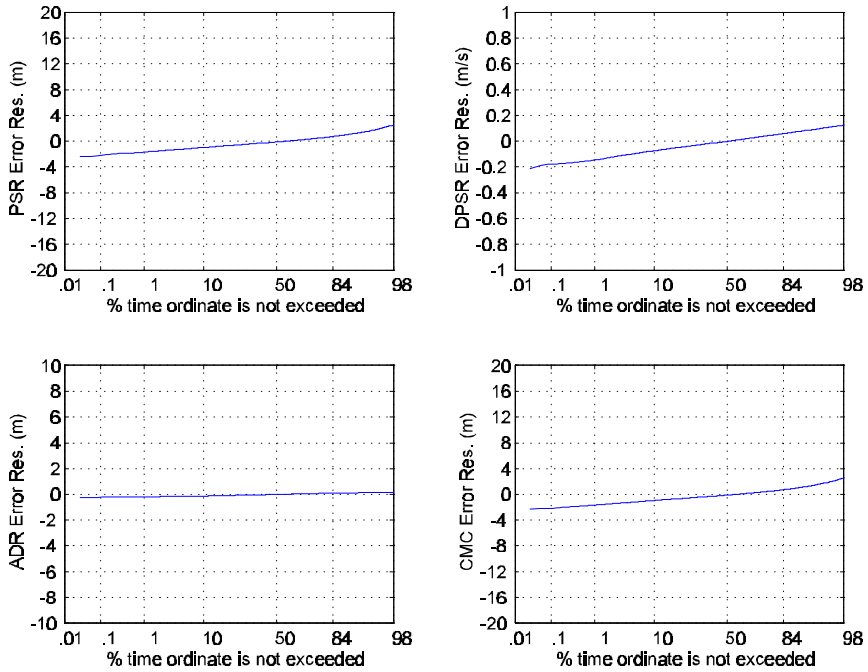

Figure 5.3.1.10 Reference range error residual CDF.

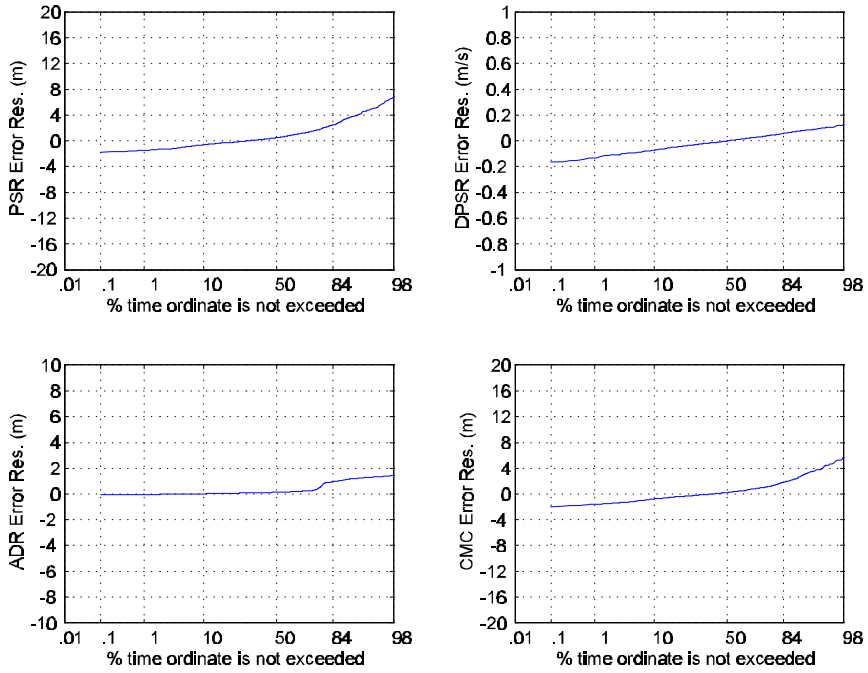

Figure 5.3.1.11 Range error residual CDF for 1-MHz PRF with UPS interference measurement.

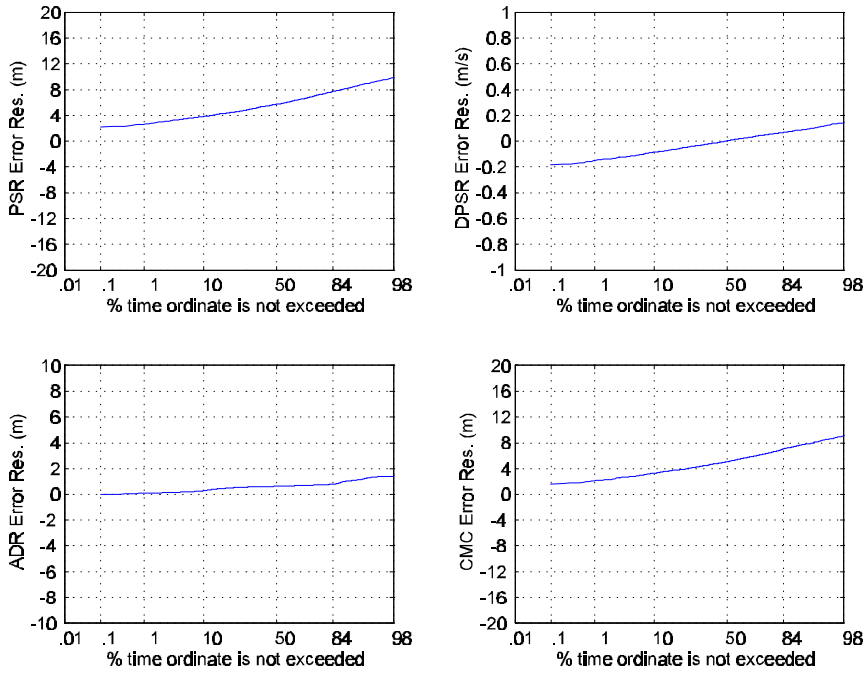

Figure 5.3.1.12 Range error residual CDF for 1-MHz PRF with 2% RRD interference measurement.

Gaussian distributed random variables have a skewness of 0. The excess measures the "peakedness" of a random variable and is defined by

$$\beta_2 = \frac{1}{\sigma^4}\sqrt{\frac{1}{N}\sum_{n=1}^{N}(\gamma_n - m_\gamma)^4} \quad .$$

Gaussian distributed random variables have an excess of 3. A Gaussian distributed random variable has a median-to-mean ratio of 1. For display, 3 is subtracted from excess and 1 is subtracted from the median-to-mean ratio so they, like skewness, will be centered at zero. Deviations from zero for any of these statistics will indicate that the random variable is non-Gaussian.

Range error residual standard deviation estimates are unreliable if there are too few independent samples. The auto-correlation function is used to evaluate the independence of the range error residual samples:

$$R_\Gamma(k) = \sum_{n=1}^{N}(\gamma_n - m_\gamma)(\gamma_{n+k} - m_\gamma) \quad ,$$

where m_ℓ represents the mean residual error and N is the number of residual error samples. The number of correlated samples is the smallest value of k whose autocorrelation is less than $R(0)/2$. ADR error residuals were typically highly correlated because ADR is the result of integrating DPSR. Figures 5.3.1.13, 5.3.1.14, and 5.3.1.15 show the autocorrelation function of the reference measurement, UPS case, and 2% RRD case. The reference measurement and 2% RRD case show clear independence between observations. The UPS case shows more correlation corresponding to the length of time spent with and without line interference.

5.3.2 Cycle Slip and Signal-to-Noise Ratio

To our knowledge, the receivers that were tested do not count or estimate the actual number of cycle slips. Instead, the receivers monitor parameters that are correlated to cycle slip conditions (e.g., SNR, carrier phase lock, and bit error rates).

Cycle slip condition is a binomially distributed random variable, being either present or not. Analysis consists of counting the number of observations where cycle slip conditions are present and dividing by the total number of observations. This fraction represents cycle slip condition probability which is converted to percentage for display.

Figures 5.3.2.1a and 5.3.2.2a show cycle slip condition probability for the two 1-MHz PRF cases described above. The UPS case has the majority of cycle slip conditions clustered around the time when line interference is strongest. For the 2% RRD case, cycle slip conditions are scattered uniformly throughout the entire measurement.

SNR is analyzed in percentiles in a similar manner to the range error residual. The occurrence of low SNR is of interest thus the 50th, 16th, and 2nd percentiles are displayed. Figures 5.3.2.1b and 5.3.2.2b show SNR behavior for the two 1-MHz PRF cases. As expected, the UPS case has degraded SNR around the time when line interference is strongest. The 2% RRD case has small degradations in SNR throughout the entire measurement.

It should be noted that GPS receiver SNR measurements may not be accurate when the band-limited UWB signal has non-Gaussian statistics. The designer of the GPS noise measurement circuitry may have assumed, for example, that the noise would have Gaussian statistics. Thus, the SNR threshold for cycle slip conditions may need to be adjusted for non-Gaussian noise.

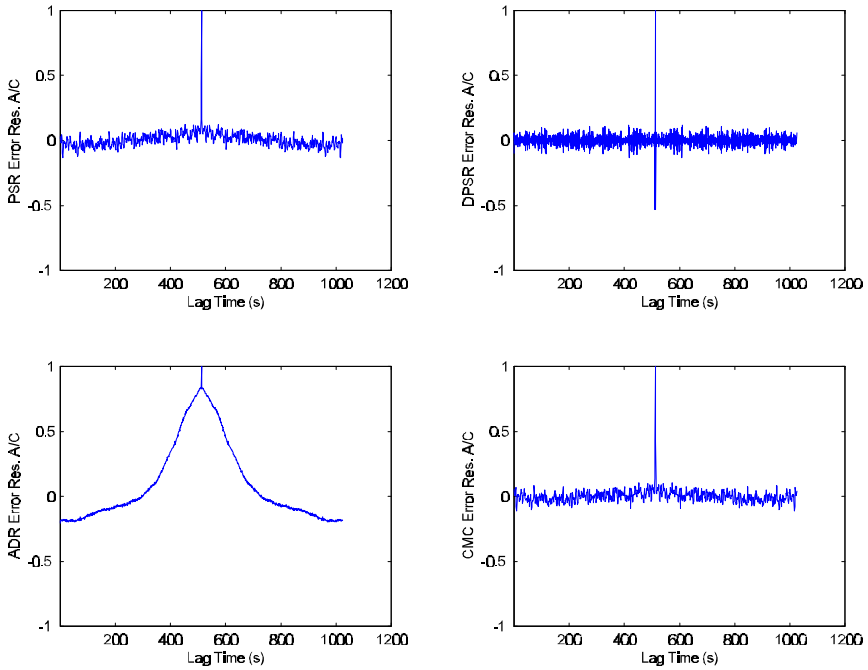

Figure 5.3.1.13 Autocorrelation of reference range error residual.

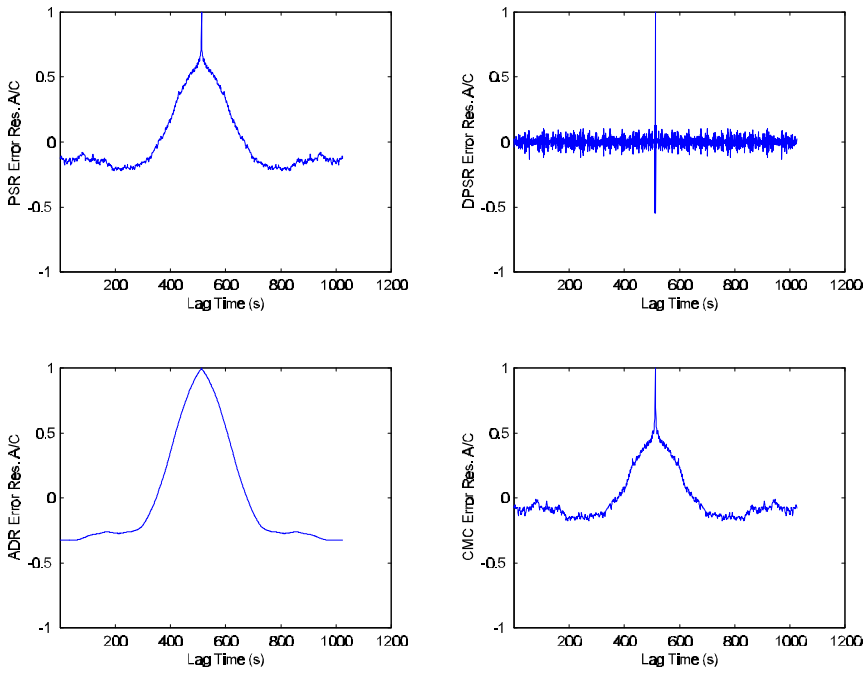

Figure 5.3.1.14 Autocorrelation of range error residual for 1-MHz PRF with UPS interference measurement.

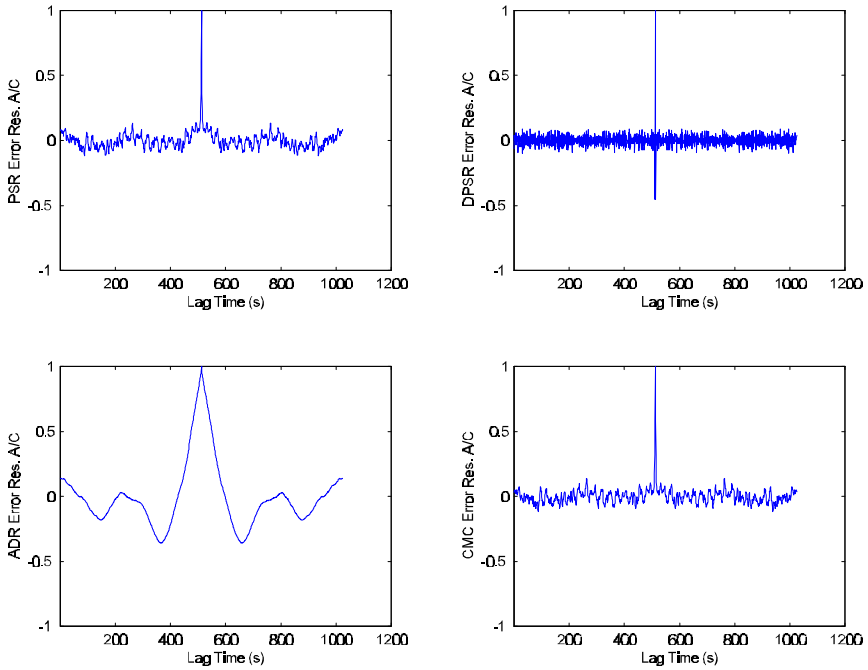

Figure 5.3.1.15 Autocorrelation for 1-MHz PRF with 2%-RRD interference measurement.

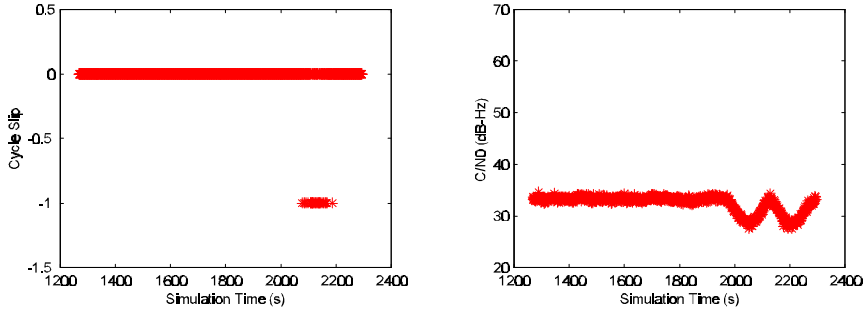

Figure 5.3.2.1 Cycle slips and SNR for 1-MHz PRF with UPS interference measurement.

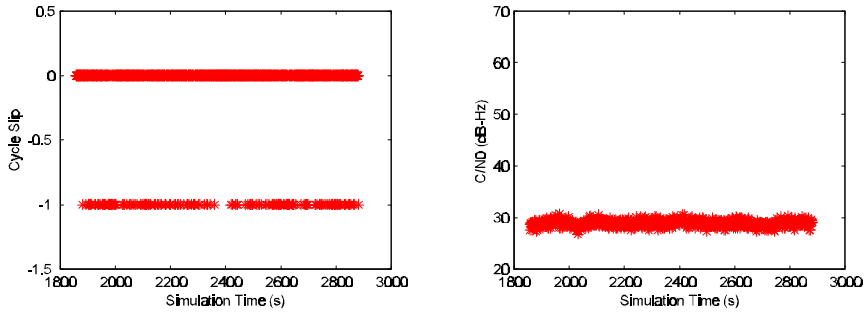

Figure 5.3.2.2 Cycle slips and SNR for 1-MHz PRF with 2%-RRD interference measurement.

5.4 Uncertainty Analysis

Four random variables are estimated through measurement: BL point, RQT, range error, and probability of cycle slip conditions. Discussion of the uncertainty of these estimates is as important as the estimates themselves.

Uncertainty is often quoted in terms of accuracy and precision. An accurate estimate implies that the mean is close to the true value. A precise estimate implies that the variation about the mean is minimal. Another way of expressing uncertainty is to define a random interval along with a probability or confidence that the random interval will include the true value [8].

5.4.1 Break-lock Point

BL point was found to occur as much as 4 dB below the UWB signal level that first caused BL. A test using Gaussian noise with Rx 1 showed that it was possible to have successful and unsuccessful BL measurements over a 4-dB range. Below this range BL was seldom experienced with repeated trials. Above this range BL was frequently experienced with repeated trials. Thus, it can be said that the BL point variability is approximately ±2 dB.

5.4.2 RQT

RQT is assumed to be Gaussian distributed. However, since there are a limited number of RQT trials the Student-t distribution is used for computational purposes. Formally, if the number of trials is fixed at 10, the confidence interval for 95% confidence is

$$m - 0.76s \le u < m + 0.76s \quad ,$$

where u is the true mean, m is the measured mean, and s is the measured standard deviation. This uncertainty estimate is only valid when all trials had successful reacquisitions. RQT trials are considered independent because the receiver was reset at the beginning of each measurement.

5.4.3 Range Error

The standard deviation of the range error residual, σ_{uere}, (user-equivalent range error) is an important factor in the GPS error budget. The uncertainty of a laboratory estimate of σ_{uere} is often expressed as a confidence interval. If there are 1024 independent observations and the underlying process is Gaussian distributed, the standard deviation interval for 95% confidence is

$$0.9585s \le \sigma < 1.045s \quad ,$$

where *s* is the measured range error residual standard deviation, and σ is the true range error residual standard deviation. Range error residual confidence intervals cannot be computed for UWB signals with spectral line interference because their statistics are non-Gaussian.

5.4.4 Cycle Slip Conditions

For Rx 1, cycle slip conditions do not cause loss of lock. Thus it was possible to collect a number of cycle slip condition samples during a single BL measurement. Although it is practical to compute the uncertainty of this random variable it is unclear how independent the cycle slip condition samples are. For example, if the cycle slip condition is detected with a message parity error it may take several seconds to clear the cycle slip condition indicator. Since cycle slips condition is used to support other trends it was deemed unnecessary to analyze the uncertainty of cycle slip condition probability.

6. RESULTS

This section discusses the measured characteristics of the various UWB interference sources, explains measured GPS operational and observational parameters, and summarizes trends.

6.1 UWB Spectral and Temporal Characteristics

In order to better understand the interference effects of UWB signals, it is helpful to understand their frequency and time-domain characteristics. A general description of the spectral features was given in Section 4.1.2. In this section, time-domain characteristics of the interfering signals are discussed.

When a narrow pulse, with a wide bandwidth (BW), is passed through a filter with a narrower bandwidth, the output is essentially equal to the impulse response of the filter and has a pulse width approximately equal to the reciprocal of the receiver bandwidth. Figure 6.1.1 illustrates 50%-ARD UWB signals, at three different PRFs, passed through a 20-MHz bandpass filter (center frequency of 1575.42 MHz) and downconverted to a center frequency of 321.4 MHz. The result is that, as the pulse passes through the filter, it becomes wider, the peak-to-average power decreases, and depending upon the PRF and extent of dithering, the pulses may overlap.

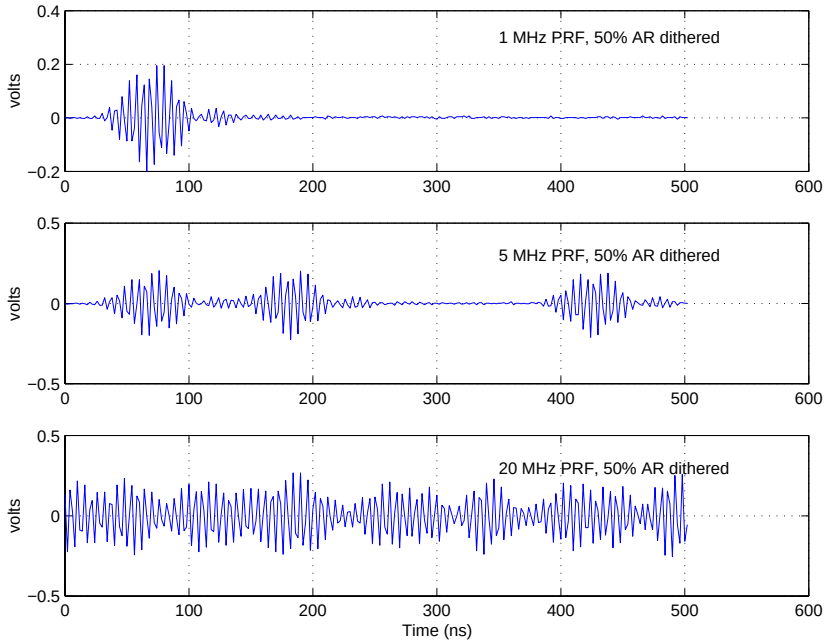

Figure 6.1.1. Temporal plots of 50%-ARD UWB signals passed through a 20-MHz bandpass filter and downconverted to a center frequency of 321.4 MHz.

One way to describe the time-domain characteristics is through APDs. These distributions are helpful for several reasons: when normalized to mean power, they can quickly show the relationship between peak, mean, and median power levels (as well as other percentiles); they reflect impulsiveness of the signal and the extent to which the signal power is present; they indicate the degree to which a signal is Gaussian; and they quickly distinguish signals that are constant amplitude in nature. APDs are particularly valuable, therefore, for providing statistical descriptions of wide bandwidth signals as they pass through the varying bandwidths of receivers. A tutorial on APDs is provided in Appendix E for those readers unfamiliar with their use.

A complete set of APDs, for each of the UWB signals used in these measurements, is provided in Appendix B. Additionally, a few composite APD plots are shown here for the purpose of illustration. For each of the composite plots, the mean power is normalized to 0 dBm so that the peak-to-average power can be readily determined. As a reference, an equivalent 0-dBm mean-power APD for Gaussian noise is plotted along with the UWB signals.

Figure 6.1.2 shows the normalized APDs for 8 different permutations of a UWB signal with a 100-kHz PRF. One can see that the amplitude distributions of the dithered signals are identical to the non-dithered cases. This is because, even for 50% ARD, the space between pulses is no less than 5 µs apart; since the UWB pulse width after passing through a 3-MHz filter is approximately 300 ns, the pulses remain discrete and never overlap.

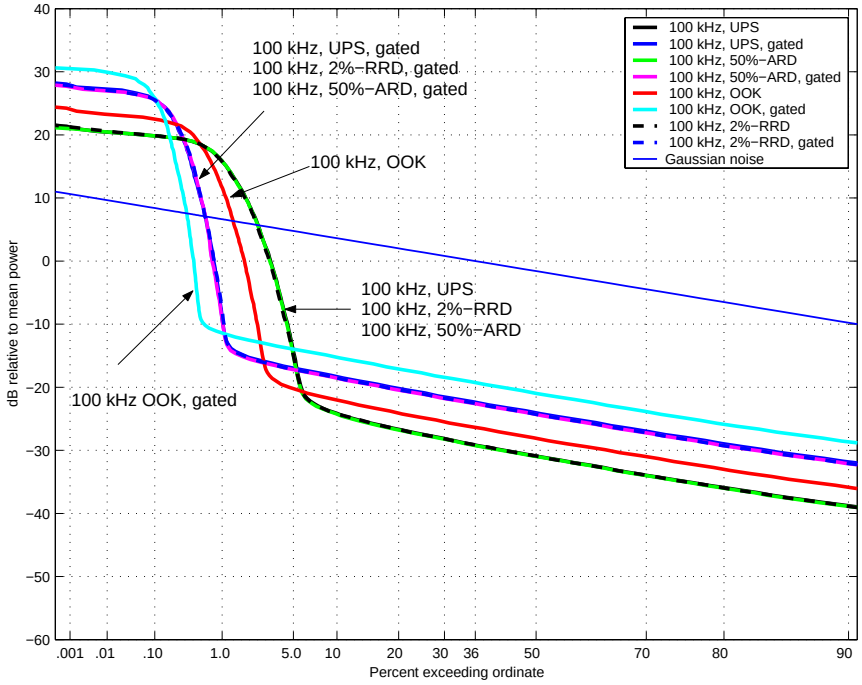

Figure 6.1.2. APDs of 100-kHz-PRF UWB signals measured in a 3-MHz bandwidth.

Therefore, while these dithered cases show a noise-like spectrum, they are non-Gaussian and impulsive with regard to their amplitude distributions.

Figure 6.1.3 shows the same plots for UWB signals with a PRF of 20 MHz. In this case, the UPS signal is sinusoidal (flat line), as we would expect since only one spectral line is allowed to pass through the 3-MHz filter. The dithered, non-gated cases, however, are Gaussian distributed. This is because the 20-MHz PRF is high enough to cause pulse overlap. Therefore, any random variations in the pulse spacing results in destructive and constructive addition of adjacent pulses and an apparent Gaussian distribution.

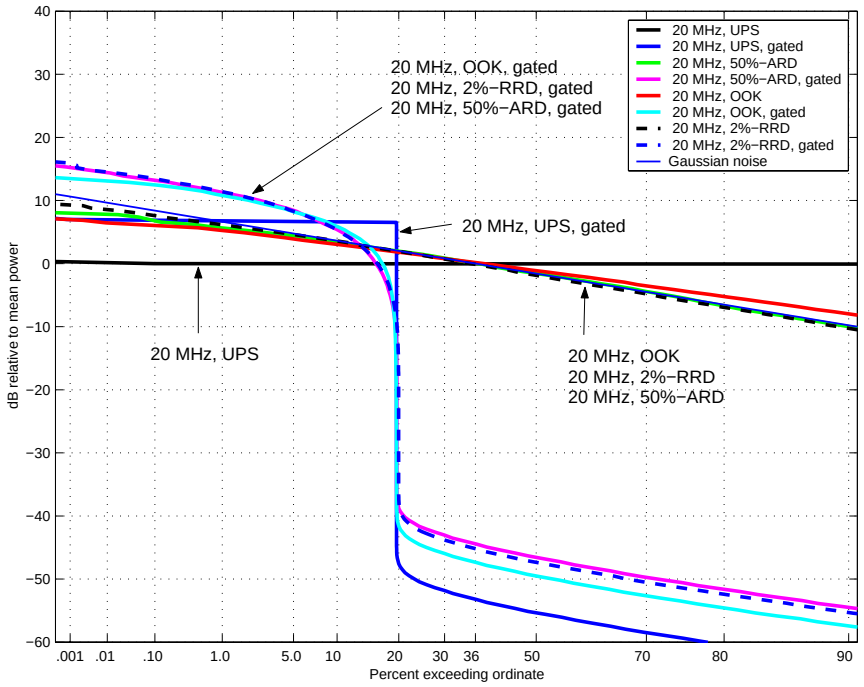

Figure 6.1.3. APDs of 20-MHz-PRF UWB signals measured in a 3-MHz bandwidth.

Figure 6.1.4 shows variations in amplitude distributions for 50% ARD pulses, varied with regard to PRF and passed through a 3-MHz bandwidth filter. One can see a natural progression as the pulses become more closely spaced: the pulse energy is present a greater percentage of the time, and as the pulses start to overlap, the signal amplitude distribution becomes more Gaussian-like.

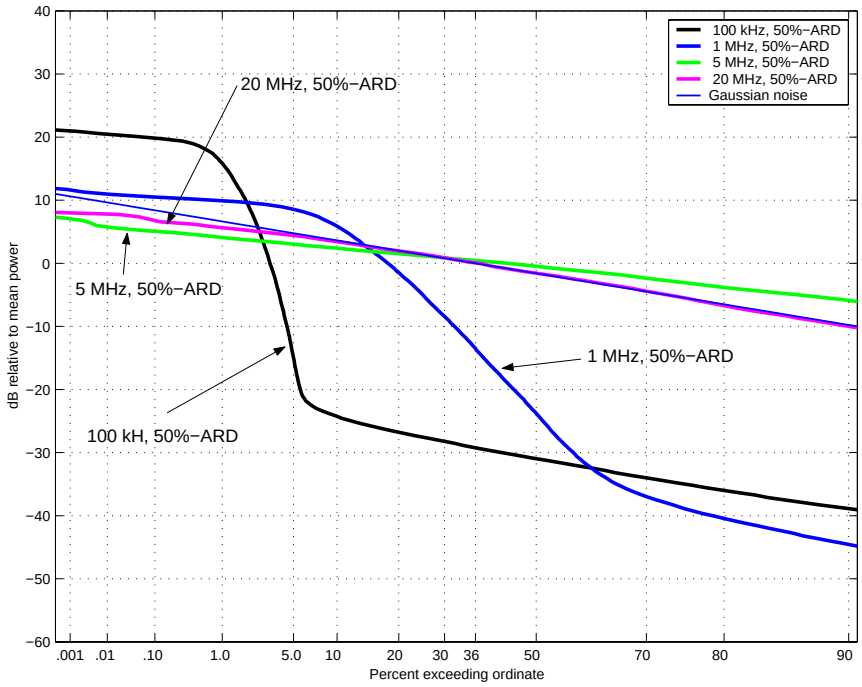

Figure 6.1.4. APDs of 50%-ARD UWB signals measured in a 3-MHz bandwidth.

6.2 GPS Interference Measurement Results

As discussed in the data analysis section, certain operational and observational metrics were chosen to demonstrate GPS receiver performance degradation. Results are given to establish how receivers respond to increasing levels of Gaussian noise with no UWB interference. Composite single-source and aggregate UWB results are provided to relate trends in GPS performance degradation to UWB interference parameters (e.g., PRF, pulse spacing). Whenever relevant, gated UWB results are plotted directly below non-gated UWB results to demonstrate the effects of gating. Table 6.2.1 gives a summary of the Figures under discussion in this section.

Table 6.2.1. Composite Figure List

Interference	Rx 1			Rx 2		
	BL	RQT	CMC	BL	RQT	CMC
Noise	6.2.1.1, 6.2.1.2	6.2.1.8	6.2.2.1	6.2.1.3, 6.2.1.4	6.2.1.8	N/A
UPS	6.2.1.1, 6.2.1.2	N/A	6.2.2.2	6.2.1.3, 6.2.1.4	N/A	N/A
OOK	6.2.1.1, 6.2.1.2	N/A	6.2.2.3	6.2.1.3, 6.2.1.4	N/A	N/A
2%-RRD	6.2.1.1, 6.2.1.2	6.2.1.9	6.2.2.4	6.2.1.3, 6.2.1.4	6.2.1.11	N/A
50%-ARD	6.2.1.1, 6.2.1.2	6.2.1.10	6.2.2.5	6.2.1.3, 6.2.1.4	6.2.1.12	N/A
Aggregate	6.2.1.7	6.2.1.13	6.2.2.6	N/A	N/A	N/A

Figures 6.2.1 through 6.2.5 are composite graphs showing the BL point for each of the UWB permutations. For those cases where no BL point is displayed, the receiver never lost lock. RQT results are given in Figures 6.2.6 through 6.2.11. CMC residual-error standard deviation was chosen to demonstrate UWB interference effects and is plotted in Figures 6.2.12 through 6.2.16.

In addition, Appendix F provides a comprehensive set of plots – each set summarizing results for type of UWB interference to a specific receiver. The plots on the left side pertain to the code-tracking loop and display CMC statistics (recall that CMC statistics are dominated by PSR statistics). Error-residual percentiles and standard deviation are shown on the upper left, and measures to quantify skewness, excess, and independence are given on the lower left. The upper-right plots provide information pertaining to carrier-loop tracking such as ADR percentiles and cycle slip conditions. Often, cycle slip conditions correlate to SNR estimated by the receiver. SNR percentiles are given with RQT data on the lower right.

The various graphs show parameter effects as a function of signal power for each of the UWB permutations. The reader is referred to Table 4.1.1 for Gaussian noise power level settings for each receiver. Also the power of all gated signals is expressed as the average power during the on-time of the gated cycle.

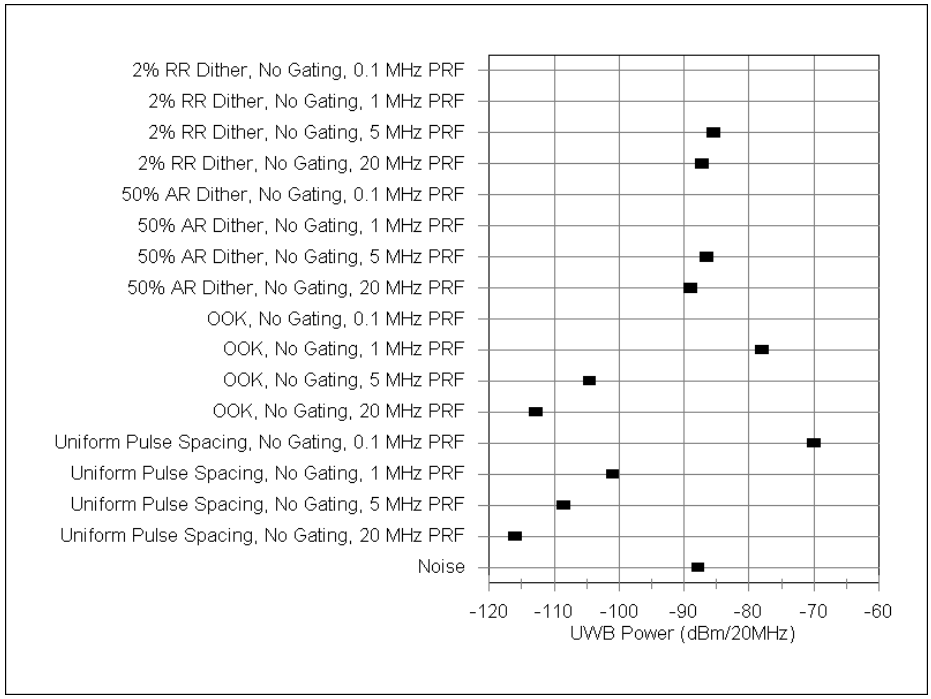

Figure 6.2.1. Non-gated UWB signal vs. signal power at BL (Rx 1).

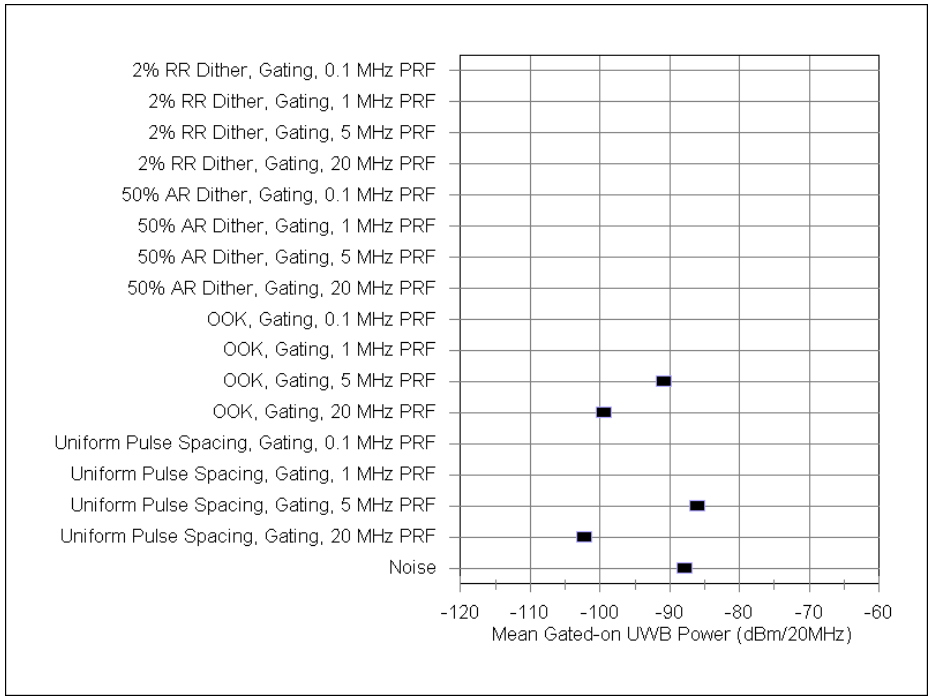

Figure 6.2.2. Gated UWB signal vs. signal power at BL (Rx 1).

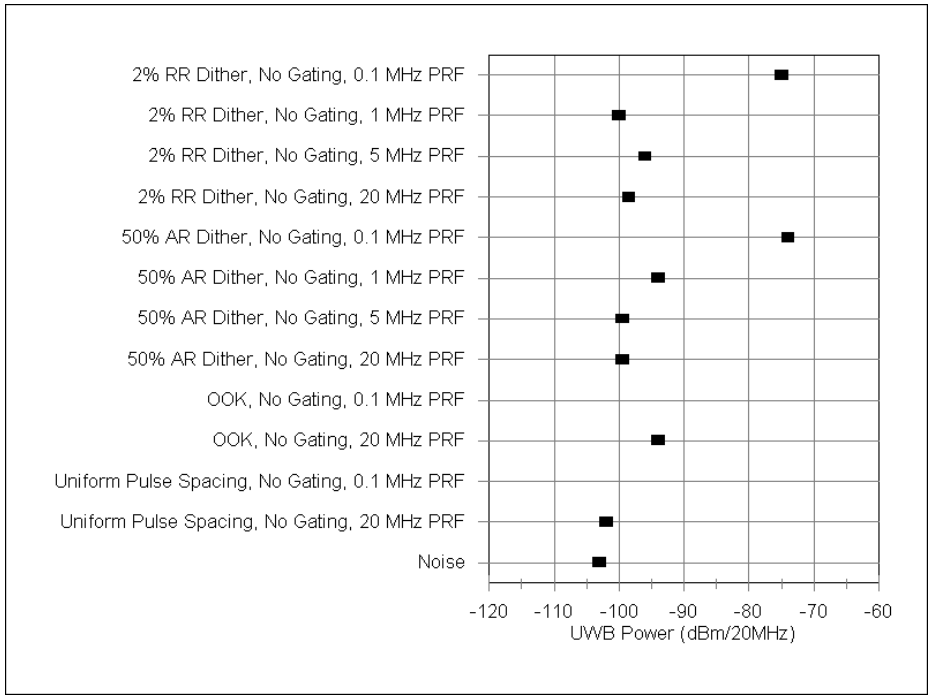

Figure 6.2.3. Non-gated UWB signal vs. signal power at BL (Rx 2).

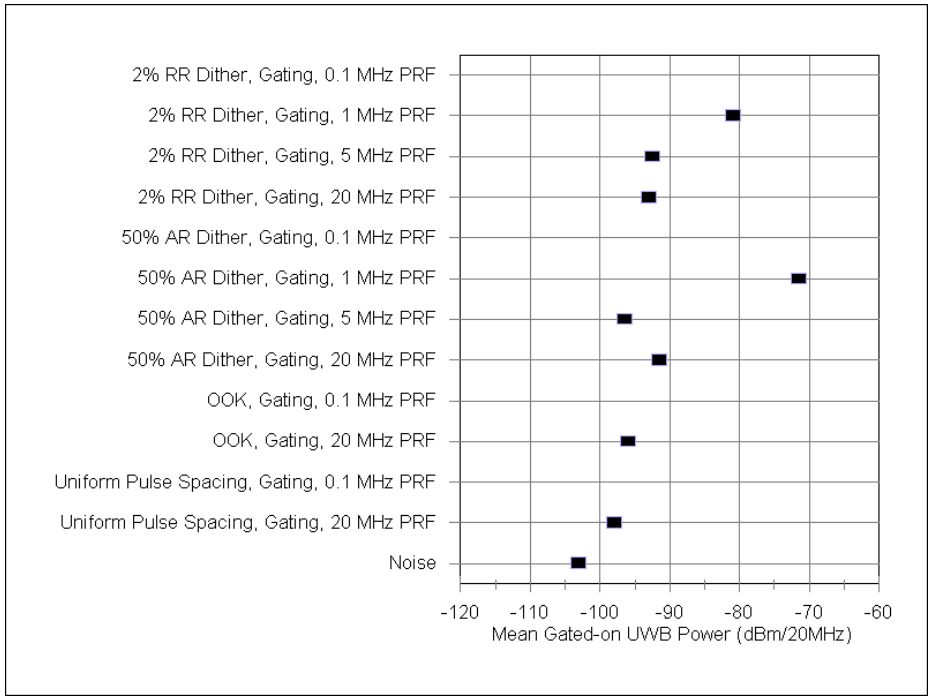

Figure 6.2.4. Gated UWB signal vs. signal power at BL (Rx 2).

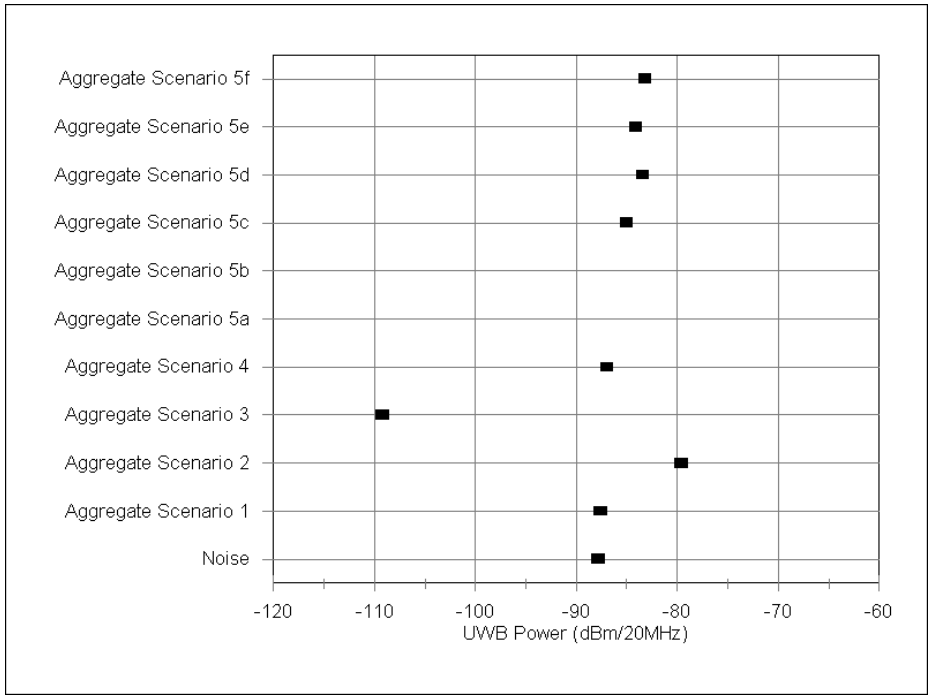

Figure 6.2.5. Aggregate UWB signal vs. signal power at BL (Rx 1).

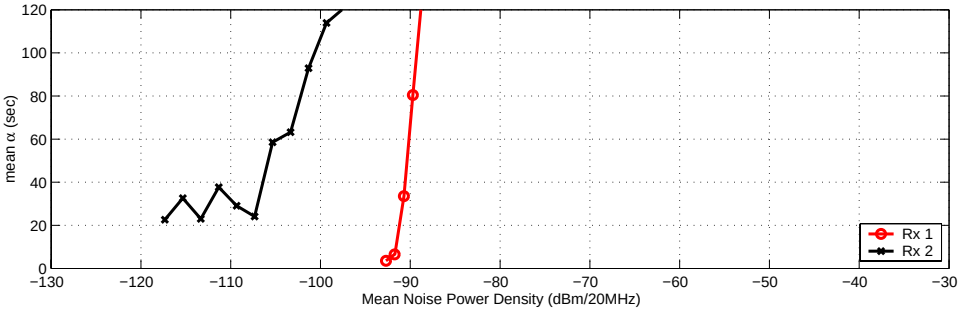

Figure 6.2.6. RQT of GPS receivers when exposed to Gaussian-noise interference.

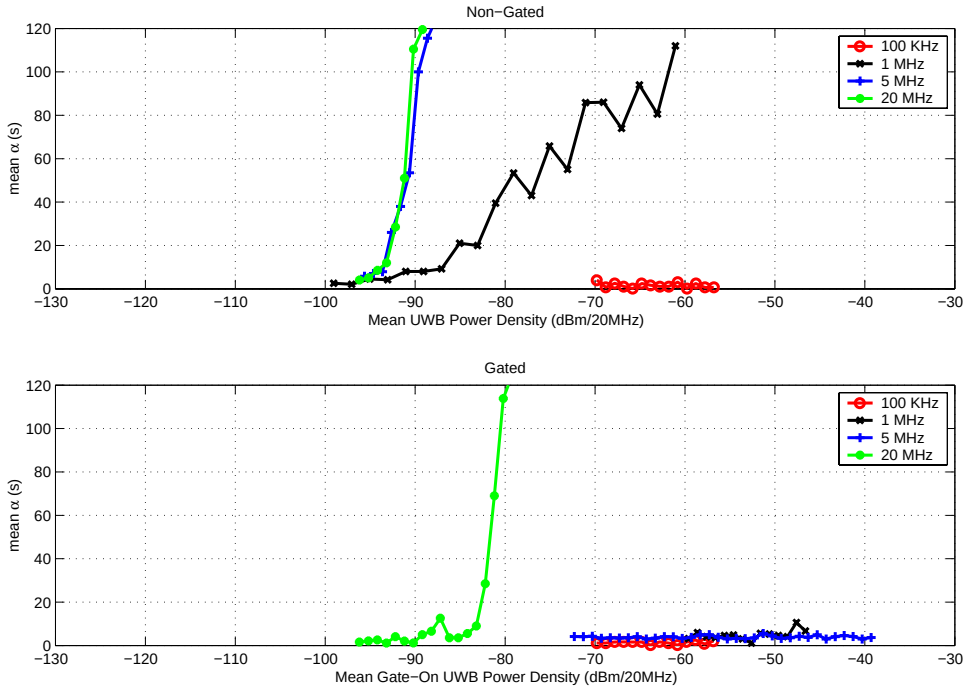

Figure 6.2.7. RQT of Rx 1 when exposed to 2%-RRD UWB interference.

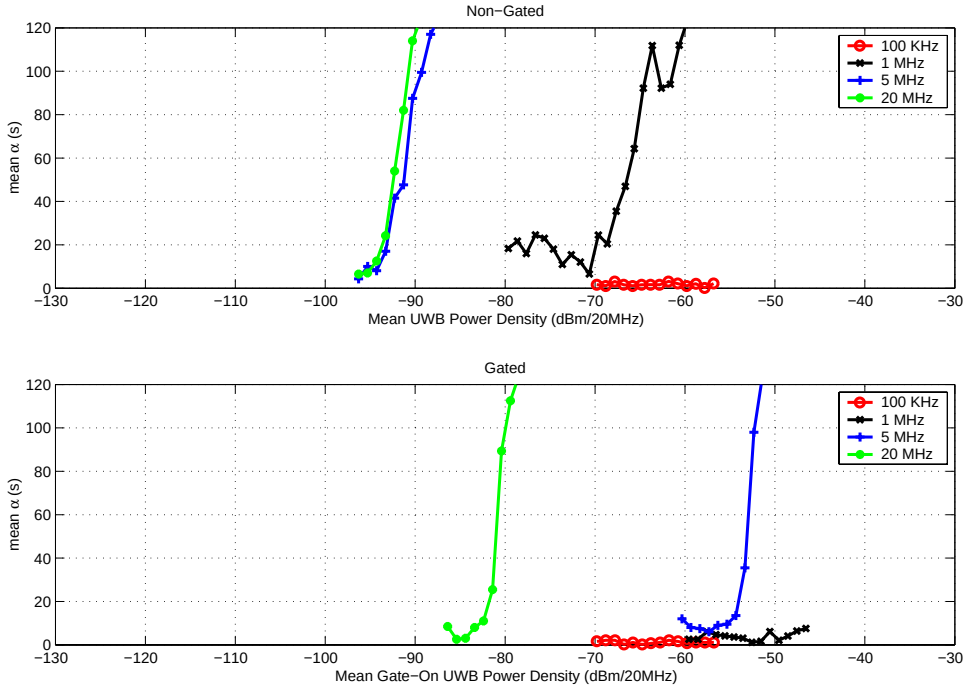

Figure 6.2.8. RQT of Rx 1 when exposed to 50%-ARD UWB interference.

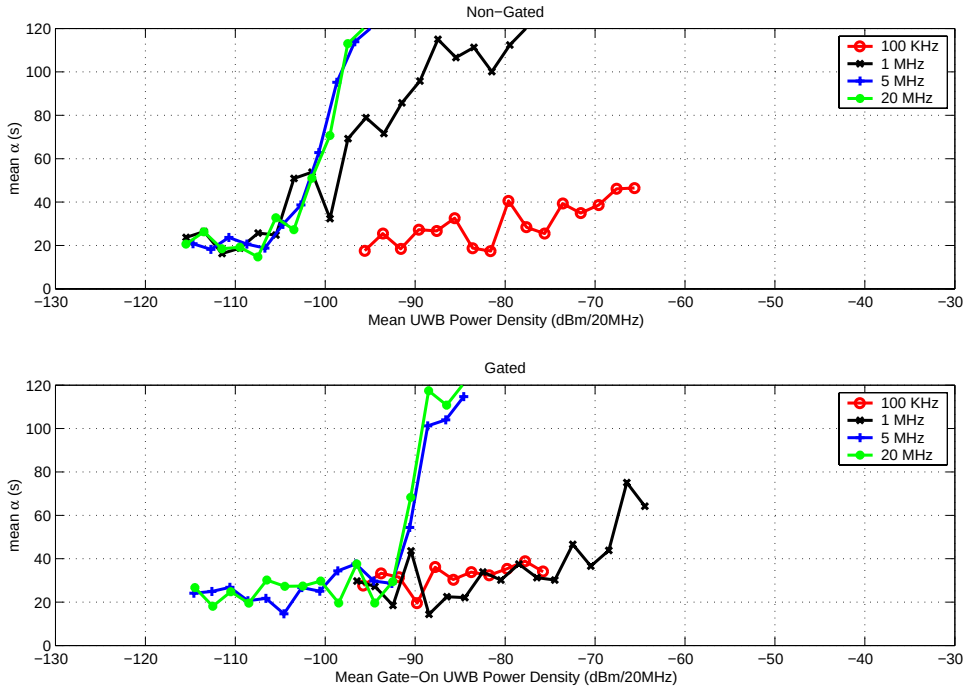

Figure 6.2.9. RQT of Rx 2 when exposed to 2%-RRD UWB interference.

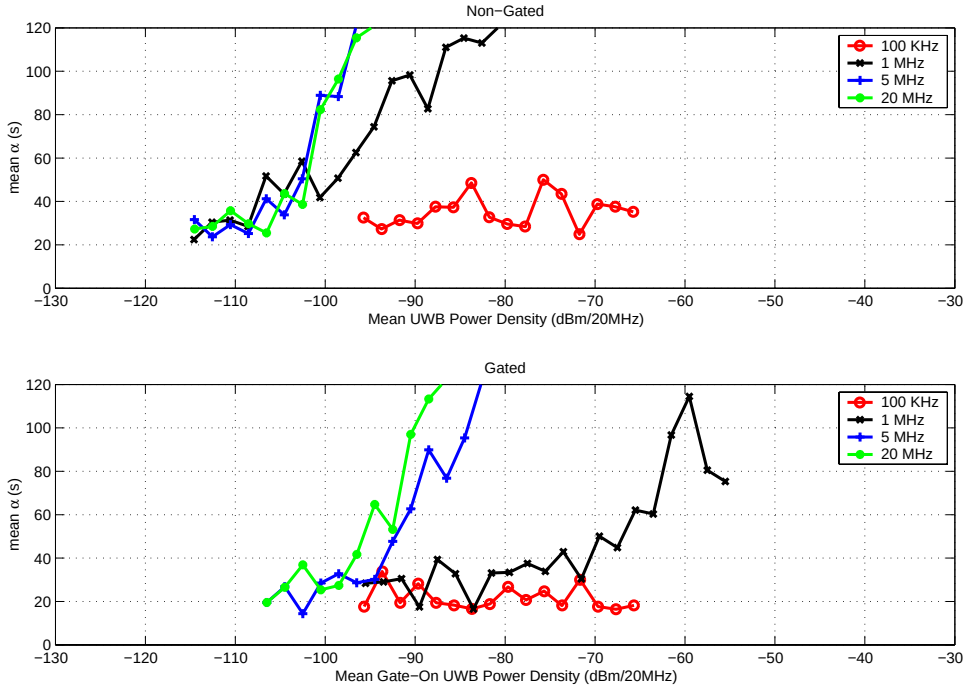

Figure 6.2.10. RQT of Rx 2 when exposed to 50%-ARD UWB interference.

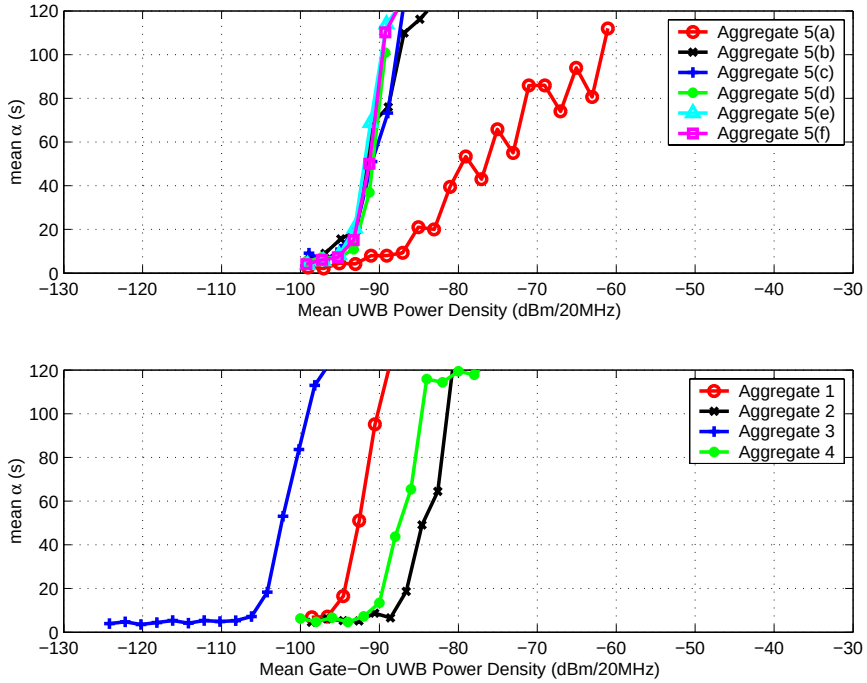

Figure 6.2.11. RQT of Rx 1 when exposed to aggregate UWB interference.

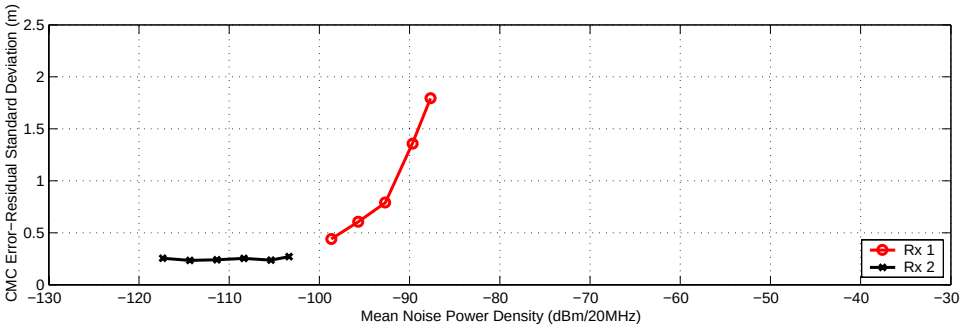

Figure 6.2.12. PSR accuracy of GPS receivers when exposed to Gaussian-noise interference.

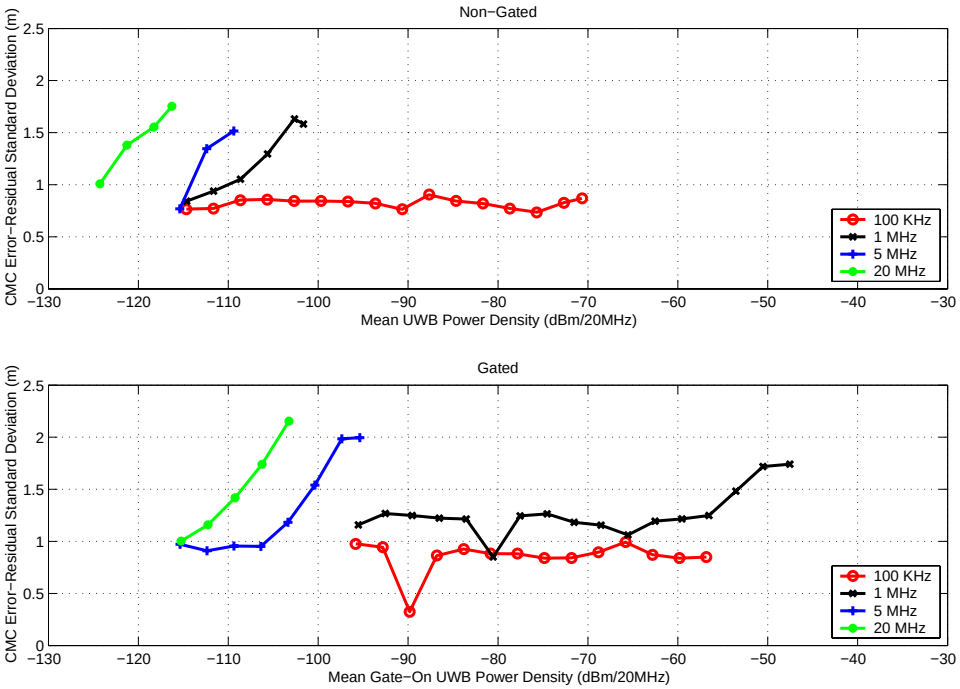

Figure 6.2.13. PSR accuracy of Rx 1 when exposed to UPS UWB interference.

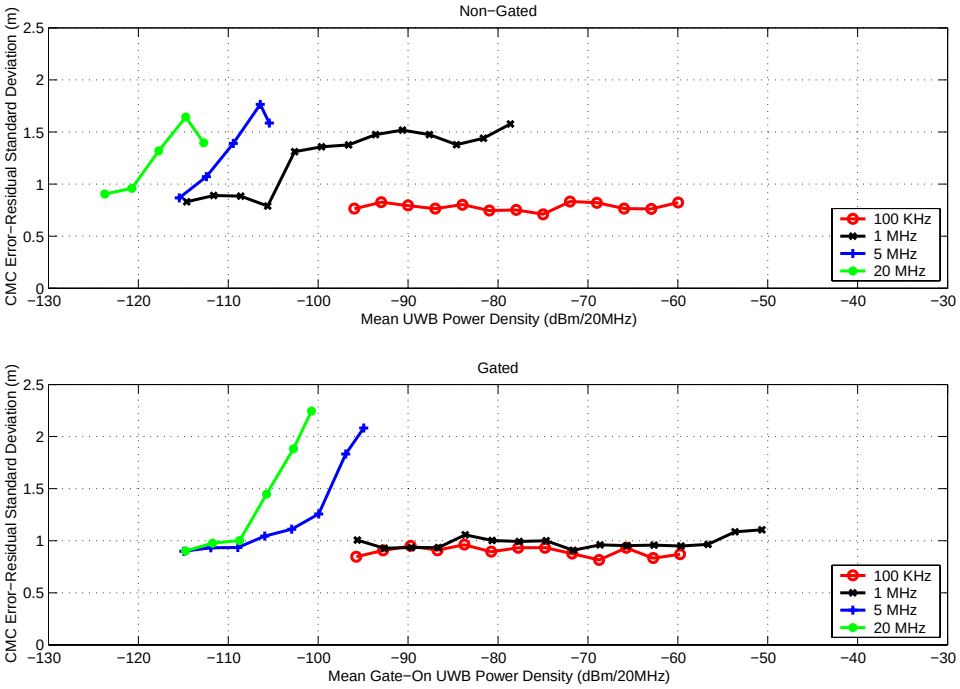

Figure 6.2.14. PSR accuracy of Rx 1 when exposed to OOK UWB interference.

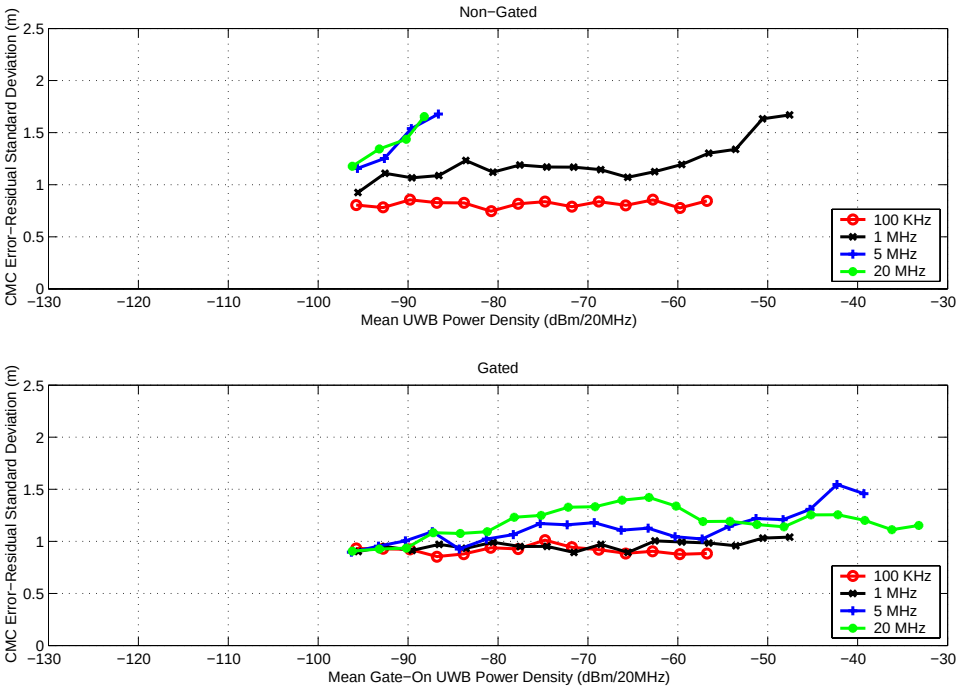

Figure 6.2.15. PSR accuracy of Rx 1 when exposed to 2%-RRD UWB interference.

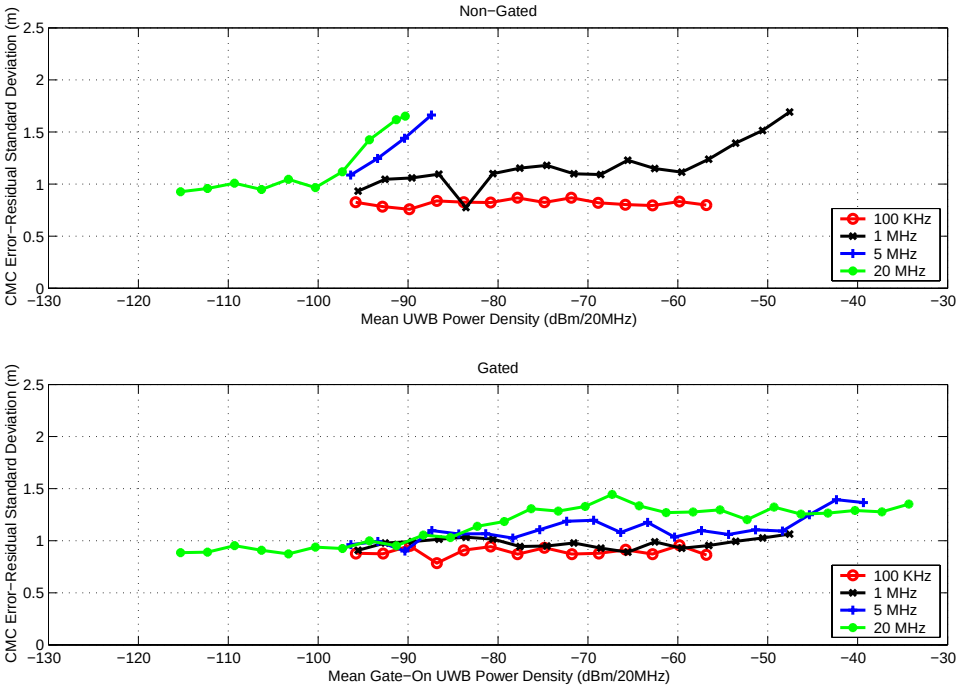

Figure 6.2.16. PSR accuracy of Rx 1 when exposed to 50%-ARD UWB interference.

6.3 Summary of Measurement Results

Because of the different receiver bandwidths and different signal processing techniques employed, each receiver responds in a different manner. In addition, there are certain trends in receiver response to UWB interference which can be identified and related to various characteristics of the UWB signals. In this section, these trends will be summarized for both receiver differences and variation in UWB signal interference.

6.3.1 Receiver Observations

Receiver 1 is a general purpose navigation receiver. Receiver 2 is a high-precision, semi-codeless receiver which relies heavily upon carrier phase information. It also has narrow correlator capabilities, and therefore wide bandwidths. It should be noted that Rx 2 was tested without the Gaussian-noise source, except for the Gaussian-noise interference test.

Several general observations can be made with respect to each receiver:

1. Figures 6.2.1 through 6.2.4 show that Rx 1 BL points occur at higher UWB signal powers for ARD and RRD, and Rx 2 showed BL at higher UWB signal powers for OOK and UPS.
2. As exemplified in Figure 6.2.6 and throughout the RQT results (e.g., Figures 6.2.7 through 6.2.10), the same RQT generally occurs at a higher interference power for Rx 1 than Rx 2.
3. Figures F.2.1 through F.2.33 show that Rx 1 is much more tolerant of cycle-slip conditions.
4. For most of the lower PRF cases (1-MHz and 0.1-MHz PRF), Rx 1 reported no change in C/N_0 despite the fact that UWB interference power was as much as 50 dB above the added Gaussian noise. This was also seen for Rx 2 for all UWB signal power levels and types.
5. Sometimes the receivers were able to reacquire at UWB signal power levels greater than the BL point (see Figures F.1.36, F.2.1, F.2.10 through F.2.15, F.2.18, F.2.19, F.2.21, F.2.22). This occurred more frequently with Rx 2.

From these and other observations, several conclusions can be drawn:

6. Because of its intended application, BL occurred for Rx 2 whenever there are cycle slips.
7. BL results show that Rx 2 is more tolerant of interference with spectral lines.
8. Reacquisition can sometimes occur at UWB power levels greater than the BL point for two reasons. One reason is that the BL point is probabilistic and can occur over a range of power levels from one time to the next. The other reason is that BL measurement duration is long, while maximum RQT is relatively short.
9. For Rx 1, the observational results are correlated to BL and RQT. For many of the UWB signals, CMC, ADR, cycles slips, and C/N_0 show significant changes and parellel RQT as the UWB interference power levels approached the BL point. However, for Rx 2 only RQT showed change prior to the BL point.

4. RQT has been found to be the most sensitive parameter for identifying interference effects on the receiver. In fact, sometimes RQT is elevated when UWB power levels are as much as 10 to 20 dB below the BL point (see Figures F.1.19, F.1.20, F.1.22, F.1.27, F.1.30, F.1.38, F.1.39, and F.2.20).

6.3.2 Variations Due to UWB Signal Characteristics

Aside from receiver differences, there are trends in receiver response related to the characteristics of the UWB signals themselves, such as pulse spacing, PRF, gating, and the accumulation of multiple UWB signals.

Pulse Spacing

Receiver effects can be directly related to the different modes of pulse spacing – UPS, dithering, and OOK. Any time the UWB signal has a uniform pulse spacing, there are spectral lines, and when these spectral lines lie within the GPS band, there is potential for alignment with spectral lines of the GPS signal. This alignment is particularly invasive as evidenced by BL at low UWB powers in Figures 6.2.1 and 6.2.2. Particularly for higher PRFs, where more power is gathered up into each of the spectral lines, Rx 1 breaks lock at power levels as much as 25 dB below the added noise. The same trends can be seen for CMC and ADR error-residual, and cycle slips.

On-off-keying, since it too has spectral lines, can have a significant impact on GPS receivers. This is evident in Figures 6.2.1, and 6.2.2, where for higher PRFs the BL point occurs by as much as 20 dB below the added noise. However, the effects of OOK are less detrimental than for UPS; this is because the spectral power is distributed between spectral lines and a noise component (see Appendix D). Also, as evidenced by comparing UPS with OOK in the APDs, OOK has the effect of increasing the peak-to-average noise power and decreasing the percentage of time the signal is present above the system noise, thus decreasing the impact on receiver performance.

Dithering reduces the impact of UWB interference on GPS receivers. As discussed in Section 4.1.2, dithering can reduce or eliminate spectral lines – thus spreading the power over the band and reducing the effects of interference. As evidenced by APDs such as those shown in Figures C.3.10 and C.3.12, UWB signals at high PRF rates (e.g., 5 and 20 MHz) are distributed similarly to Gaussian noise when limited to a 3-MHz bandwidth. This is in keeping with the BL results shown in Figures 6.2.1 through 6.2.4, where for higher PRFs, dithering shows BL results similar to Gaussian noise. For the lower PRFs of 1.0 and 0.1 MHz, the impact from dithered UWB signals is even further reduced.

Pulse Repetition Frequency

Higher PRFs have a greater detrimental effect for two reasons. One is that for those cases with spectral lines, greater power is gathered into each spectral line. The other reason is that higher PRFs result in a reduced peak to average power ratio and a greater percentage of time for which the signal is present. This is evident in measured APDs such as those shown in Figure C.3.9. For each of the plots in Figures 6.2.1 through 6.2.4, one can see a natural progression of the point of BL moving to lower UWB power densities as the PRF increases, irrespective of the pulse spacing mode. The same trends can be seen for RQT, CMC and ADR error-residual, and cycle slips.

Gating

Gating reduces the impact on receivers for two reasons. One is that, as mentioned in Section 4.1.2, the power of individual spectral lines is spread out into multiple lines, thus reducing the power contained in any single line. The other reason is that, for signals of equal gated-on power density, the percentage of time the signal is present is less with gating. For each of the parameters measured, one can readily see that for the same power density during the gated-on time, the detrimental effects are significantly reduced as compared to non-gated signals.

Accumulation of Multiple UWB Signals

With the aggregate of multiple asynchronous UWB signals, one would expect the sum of the signals to become more Gaussian noise-like in its distribution and effects on GPS receivers. There are several trends which can be noted when examining the characteristics of each of the aggregate scenarios described in Table 4.1.2.2. As shown in Figures C.3.30 and C.3.31, increasing the number of summed signals in scenario 5 causes the aggregate signal to become more Gaussian – the extent being dependent upon the bandwidth. Scenarios 2 and 4 are somewhat more impulsive in nature because of asynchronous gating applied to several of the signals. Scenarios 1 and 3 both have relatively Gaussian distributions; however, scenarios 3 and 4 both have strong spectral lines – scenario 3 being potentially more invasive, in that it has more power gathered up into lines spaced 10 MHz apart.

The characteristics of these aggregate signals can be directly related to the impact on receiver performance. As noted in Figure 6.2.5, scenarios 1 and 4 show BL test results similar to noise. Scenario 2, which is essentially the same as scenario 1 but with gating applied, shows a BL point at a lower gated-on power than its non-gated counterpart. Scenario 3 shows a BL point at a low signal power because, while its APD is Gaussian distributed, it has strong spectral lines (see Figure 6.3.2.1). Scenario 5 (*a* through *f*) shows effects similar to Gaussian noise for an aggregate of anything more than 2 signals.

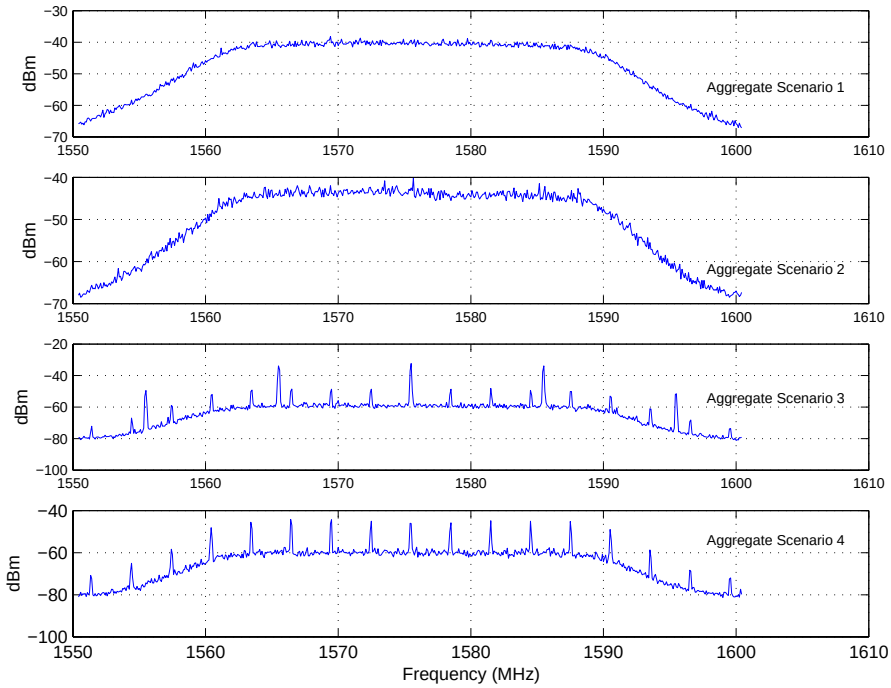

Figure 6.3.2.1. Spectral characteristics (through a 24-MHz filter) for aggregate case 1 through 4.

This Page Intentionally Left Blank

This Page Intentionally Left Blank

7. CONCLUSION

Several major studies were performed to evaluate the effect of UWB signals on GPS receiver performance. These studies characterized the UWB signals, compared conducted and radiated UWB signals, and evaluated effects of the UWB interference on GPS receiver operation (i.e. locking) and "observables."

The GPS signal was generated by a GPS constellation simulator. A select group of UWB signals were generated with a programable arbitrary waveform generator and custom hardware which triggered a sequence of UWB pulses. Signals with uniform pulse spacing (UPS), on-off-keying (OOK) , 2% relative reference dithering (RRD), and 50% absolute reference dithering (ARD) signals at 0.1, 1.0, 5.0, and 20.0 MHz pulse repetition frequencies (PRF) were used. These signals could also be gated to imitate the bursty nature of some UWB devices. Various combinations of signals were at times combined to simulate interference from multiple UWB devices.

The UWB signals were sampled and characterized with the amplitude probability distribution (APD) in hopes that APD features (i.e., constant amplitude, Gaussian noise, and impulsive noise) can be correlated to GPS receiver performance degradation. In addition, although under usual conditions, radiated UWB and GPS signals are combined at the antenna, this study uses conducted signals to maximize control and repeatability of experimental conditions. A comparison of radiated and conducted UWB-signal APDs and waveforms showed that systematic errors were not introduced by the conducted approach.

Two independent operational tests, break lock (BL) and reacquisition time (RQT), measured the receiver's ability to maintain and reacquire lock over a range of UWB signal powers. The BL and RQT metrics bracket a region of GPS receiver performance degradation. The RQT determines the lower bound where the interference begins to have a detrimental effect on the operation of the receiver. The BL point sets the upper bound where operation is impossible.

The observational test, conducted in parallel with the BL test, retrieved "observable" measurements made by the GPS receiver to estimate performance degradation. Pseudorange and carrier phase measurements were used to determine various range estimates that were compared to simulated ranges in order to evaluate the effects of UWB interference. Cycle slip indication and signal-to-noise ratio measurements evaluate the receivers ability to detect interference and make decisions regarding GPS measurement integrity.

The BL point varied most with the type of receiver. The semi-codeless receiver broke lock with the first indication of cycle slip conditions. The general purpose navigation receiver continued operation with frequent indications of cycle slip conditions. RQT was found to be the most sensitive metric. In many cases RQT showed increases without attendant degradations in range error or increases in frequency of cycle-slip conditions. RQT, range error, and cycle slip condition indicators generally show a gradual degradation as UWB signal power is increased.

This shows that the strength of the measurement methodology lies not in a single result but in the total picture painted by the combined results.

UPS and OOK signals have discrete spectral lines. Time-varying Doppler shift due to satellite motion inevitably causes these lines to interfere with GPS discrete spectral lines. These test results show that observables degrade at low UWB signal powers as the lines approach and recede. Line interference becomes more severe as PRF increases.

APDs of sampled 50%-ARD and 2%-RRD signals approach that of Gaussian noise as PRF increases. Consequently, for high-PRF dithered signals, interference effects resemble that of Gaussian noise. In general, low-PRF dithered signals generate more impulsive interference which is more benign than Gaussian noise.

8. ACKNOWLEDGMENTS

This investigation required a number of ITS engineers with a broad range of expertise and skills. The authors recognize Dr. William Kissick for his vision and leadership; Yeh Lo, John Ewan, and Wayde Allen for hardware design and production; Robert Matheson for his written contributions and insights shared; Brent Bedford for coordination of the radiated measurements; and Jeanne Ratzloff for web site development.

Steve Jones, Ed Drocella, Mark Settle, and David Anderson of the Office of Spectrum Management contributed significantly in the development of the original test plan and interpretation of the results.

Dr. Robert Johnk of the National Institute of Standards and Technology (NIST) Radio-Frequency Technology Division (Time-Domain Laboratory) is recognized for his efforts in the radiated measurements of UWB signals.

Finally, the authors recognize the 746th Test Squadron from Holloman Air Force Base for engineering support with respect to the GPS simulator.

This Page Intentionally Left Blank

This Page Intentionally Left Blank

9. REFERENCES

[1] *Notice of Proposed Rulemaking*, ET Dkt. 98-153 (rel. May 11, 2000), Federal Register, June 14, 2000, vol. 65, No. 115), pp. 37332 - 37335.

[2] W.A. Kissick, Ed., "The temporal and spectral characteristics of ultrawideband signals," NTIA Report 01-383, Jan. 2001.

[3] Recommendation ITU-R M.1477, Technical and Performance Characteristics of Current and Planned RNSS (Space-to-Earth) and ARNS Receivers to be Considered in Interference Studies in the Band 1559-1610 MHz.

[4] ARINC Research Corporation, *Navstar GPS Space Segment/Navigation User Interfaces* (Sept. 25, 1997).

[5] J.L. Leva, M.U. deHaag, and K.V. Dyke, "Performance of Stand Alone GPS," Chapter 7 of *Understanding GPS Principles and Applications*, E.D. Kaplan, Ed., Boston, MA: Artech House, 1996, pp. 237-320.

[6] P.Axelrad and R.G. Brown, "GPS Navigation Algorithms," Chapter 9 of *Global Positioning System: Theory and Applications*, B.W. Parkinson and J.J. Spilker, Eds., Washington, DC: American Institute fo Astronautics, Inc., 1996, pp. 409-433.

[7] O.L.Davies and P.L. Goldsmith, "Averages and Measures of Dispersion", Chapter 3 of *Statistical Methods in Research and Production*, O.L. Davies and P.L. Goldsmith, Eds., Tweeddale Court, Edinburgh: Oliver and Boyd, 1972, pp. 30-57.

[8] J.R. Green and D. Margerison, "Confidence Intervals," Chapter 6 of *Statistical Treatment of Experimental Data*, New York, NY: Elsevier Scientific Publishing, 1978, pp. 93-111.

This Page Intentionally Left Blank

This Page Intentionally Left Blank

10. GLOSSARY

ADR	Accumulated delta-range
APD	Amplitude probability distribution
ARD	Absolute referenced dithering
ARL/UT	Applied Research Laboratories of the University of Texas at Austin
AWG	Arbitrary waveform generator
BL	Break-lock
BPF	Bandpass filter
BW	Bandwidth
C/A Code	Coarse acquisition code
CDF	Cumulative distribution function
CDMA	Code division multiple access
CMC	Code-minus-carrier
CW	Continuous wave
DOT	Department of Transportation
DPSR	Delta-PSR
GPS	Global positioning system
FCC	Federal Communications Commission
IF	Intermediate frequency
ITS	Institute for Telecommunication Sciences
L1 band	GPS frequency band centered at 1575.41 MHz

L2 band	GPS frequency band centered at 1227.6 MHz
LNA	Low noise amplifier
LSNB	Line spreading null-to-null bandwidth – referring to the null spacing of the convolving $sinc^2$ function as a result of gating, where the null-to-null bandwidth is equal to 2 times the reciprocal of the gated-on time.
LSS	Line spread spacing – referring to the spacing between lines of the convolving $sinc^2$ function as a result of gating, where the distance between lines is equal to the reciprocal of the gating period
ND	Noise diode
NIST	National Institute for Standards and Technology
NPRM	Notice of proposed rulemaking
NTIA	National Telecommunications and Information Administration
OSM	Office of Spectrum Management
OOK	On-off keying
PDOP	Position dilution of precision
PPM	Pulse-position modulation
PRL	Pattern repetition lines – referring to spectral lines generated due to a repetition of the pulse pattern
PRF	Pulse repetition frequency
PRP	Pulse repetition period – defined as the reciprocal of PRF
PRR	Pulse repetition frequency
PRN	Pseudo-random noise
PSR	Pseudorange
P(Y) code	Encrypted high-precision pseudo-random noise (PRN) codes

RF	Radio frequency
RRD	Relative referenced dithering
RQT	Reacquisition time
RQT_{max}	The maximum time for reacquisition, after which the RQT trial is considered unsuccessful.
Rx	Receiver
SN	Spectral node – referring to a spectral feature due to the placement of the position of pulses within discrete bins
SNR	Signal-to-noise ratiow
SV	Space vehicle
Tx	Transmitter
UPS	Uniform pulse spacing
UWB	Ultrawideband – referring to ultrawideband signals
VA	Variable attenuators

This Page Intentionally Left Blank

This Page Intentionally Left Blank